University of Stavanger

Faculty of Science and Technology

BACHELOR`S THESIS

Study program/Specialization: Mechanical Engineering	Spring semester, 2021 Open / Restricted access
Writers: Sindre Fjermedal Joachim Skjervik Merenyi	Sindre Fjermedal Joachim S. Merenyi (Writers signatures)
Faculty supervisor: Hirpa Gelgele Lemu External supervisor(s): N/A	
Thesis title: Design and control of ROV manipulators	
Credits (ECTS): 2x20	
Key words: ROV, Manipulator, Subsea	Pages: 109 + enclosure: N/A Stavanger, 15/5-21 Date/year

Frontpage for bachelor thesis
Faculty of Science and Technology
Decision made by the Dean October 30th 2009

Acknowledgements

This bachelor thesis marks the finish line of our three-year long education in mechanical engineering at the University of Stavanger. These years have been both educational and challenging.

We would like to express our gratitude to all members of UiS Subsea. Covid-19 forced us to work in a completely different way than we expected. Despite the obstacles, we had a great time, and we look forward to competing this summer.

Without the support from our sponsors the project would not have been able to proceed. Even during a pandemic our sponsors saw the benefits of our project. A special thank you goes to our advisor Hirpa Gelgele Lemu and without him the project would not have been possible. The last group we would like to give our thanks to is all the employees at the UiS workshop. Without their support and practical problem solving, we would have wasted quite a few hours in the production and assembly.

Thank you all for your support during this semester.

Table of Contents

Figures

Tables

Nomenclature

Vectors are denoted with an arrow above the parameter. Example of a vector

$\vec{\imath}$

Matrices are denoted with bold capital letters. Example of a matrix

$\boldsymbol{A}$

AUV	Autonomous Underwater Vehicle
BLDC	Brushless Direct Current
CAD	Computer Aided Design
CM	Centre of mass
DC	Direct current
DH	Denavit-Hartenberg
DOF	Degrees of Freedom
FEA	Finite element analysis
ID	Inner Diameter
MATE	Marine Advanced Technology Education
MBD	Multibody Dynamics
OD	Outer Diameter
PPS	Pulses per second
PVC	Polyvinylchloride
ROV	Remote Operated Vehicle
UiS	Universitetet i Stavanger (University of Stavanger)
USB	Universal Serial Bus

A	Cross-sectional area
a_i	Displacement from previous z-axis along the current joint's axis
$\vec{a}$	Acceleration vector
C_0	Static load rating
c	Effective length factor
D	Pulley diameter
d	Shaft or bore diameter
E	Young's modulus
F	Force
f_y	Yield strength
g	Gravitational acceleration
h	Depth of bore
$i_{transmit}$	Transmission factor
k	Spring constant

L	Measured length
L_{cr}	Effective length
l_i	Displacement along the previous joint's z-axis
M_z	Torsion moment
m	Module
n	Rotations per minute
P	Pressure
p	Contact pressure
$\vec{p}$	Position vector
Q	Power output
q_i	Rotation about the previous joint's z- axis
$\boldsymbol{R}$	DH rotation matrix
r	Radius
S	Stepper resolution
T	Torque
$\boldsymbol{T}$	DH transformation matrix
v	Poisson's ratio
$\vec{v}$	Velocity vector
z	Number of teeth

α	Reference angle
α_a	Shaft influence coefficient
α_n	Bore influence coefficient
β_i	Rotation about the current joint's x-axis
γ	Lead angle
Δx	Change in length
δ	Difference between shaft and bore diameter
η	Efficiency
θ	Joint angle
$\bar{\lambda}$	Non-dimensional slenderness
λ_1	Critical slenderness
μ	Coefficient of friction
μ_s	Static coefficient of friction
ρ	Density
σ_{cr}	Critical buckling stress
τ	Shear stress
φ	Grip angle
χ	Reduction factor
ω	Angular velocity

Summary

This thesis is about the design and production of a manipulator for a ROV for the student driven company UiS Subsea. The ROV will be used in the MATE ROV competition.

The design and mechanisms were chosen based on weight optimization, lifting capacity, and how well it can execute the tasks in the MATE competition. Autodesk Inventor was used to design all the non-standard parts and the software Adams was used to simulate the movement of the arm.

The manipulators from previous years varied from very large and heavy, to small and with limited movement. Some ideas and mechanisms were re-used and implemented into the final design of the manipulator, while other new types of mechanisms were tested from early on and selected based on efficiency and lifting capacity.

The first prototype was 3D-printed, and any visible sign of weaknesses or potential of failure was improved. This was an iterative testing phase and the result was that the final design has two main rotational joints and one rotational joint for the end effector, in total three 3 DOF.

There are 4 electrical motors in total to execute the movements of the manipulator. One motor for each main joint, one for the rotation of the end effector, and one to pull the wire for gripping. Three stepper motors are placed on the base, behind the arm. A smaller BLDC motor is placed in the arm, right behind the end effector.

Compared to manipulators from previous years, the manipulator in this thesis is much lighter while only sacrificing one DOF. Comparing to the manipulator from 2015 the new manipulator is approximately 45% lighter.

1. Introduction

Earth is often referred to as the blue planet, as 75% of the Earth's surface is covered in water either in liquid or solid form. The oceans accounts for 96.5% of this water [1] and the oceans control the climate, provides habitats, and can be used for harnessing energy.

Early exploration of the oceans was expensive and time consuming, requiring great capital. Therefore, the only industries capable of developing the early ROVs (remote operated vehicles) were the military and oil industry [2]. Humans have now explored approximately 4% of the visible universe, but despite being great space explorers, we have only explored about 5% of the oceans [3].

Correctly mapping of ocean currents, wind directions and habitats may solve some of the biggest problems our society is facing. By doing so one can use specific areas for industry and keep the most pristine habitats as reservations. A great concern for the society is plastic pollution. The oceans are becoming the world's waste dump and there is estimated to be more plastic in the oceans by 2050 than fish. Mapping of the ocean currents can provide a way to find where the waste gets piled up, and by going backwards one can find the source.

To overcome some of the challenges facing society, affordable technology must be developed. That is the mission MATE (Marine Advanced Technology Education) has set out to solve. MATE hopes to achieve this through arranging an underwater ROV competition, where students from all over the world come together to compete and solve some of the world's issues.

UiS Subsea is a student organization that was founded in 2013 to participate in MATE. The goal is for students to gain technical experience within the subsea field and promote learning. UiS Subsea have been participating in the MATE Competition every year except for 2020. The 2021 team consist of 14 electrical engineering and 4 mechanical engineering students.

If society refuses to change its path regarding pollution, perhaps the future world will look as shown in Figure 1.

Figure 1 Earth as a waste dump [4]

1.1 Objective

The objective of this thesis is best explained by the text below given by Hirpa G. Lemu.

> *The objective of this bachelor project is to develop the design of a robot manipulator for use on ROV to be built by UiS Subsea team for 2021 MATE competition.*
>
> *The manipulator is primarily designed and constructed for the tasks specified in the competition manual provided by MATE. In addition, the bachelor project involves simulation (using tools such as Adams) of a manipulator with specified degrees of freedom for underwater operations and developing adaptive control methods to ensure the effective control and operation of underwater robots.*
>
> *The project is designed for 2 students*

1.2 Terms

The most important terms used in this project will be described in this chapter. All acronyms and abbreviations are written in the short form, followed by the long form in a parenthesis first time it is written. Example: UiS (Universitetet i Stavanger). An explanation for acronyms, abbreviations and symbols is also given in the Nomenclature section.

ROV

A ROV, remote operated vehicle, is a vehicle used to access areas a human would consider to be too dangerous to enter. This may be areas exposed to nuclear radiation, fire, or subsea areas. This project is for use in subsea operations and will not consider other areas.

The pilot operating the vehicle is not located in the same place as the ROV, hence the name remote. The pilot is usually at a boat above the water surface or on land. Small sized ROVs may not require anyone other than the pilot, but larger commercial ROVs involve large teams. The teams often consist of multiple pilots, map readers, technicians, and leaders.

Orientation and movement of a ROV follows standards used in marine traffic. These terms have been used for boats in generations and it is therefore natural to continue using these. See Figure 2 for an explanation, this figure is an early sketch of the UiS Subsea ROV.

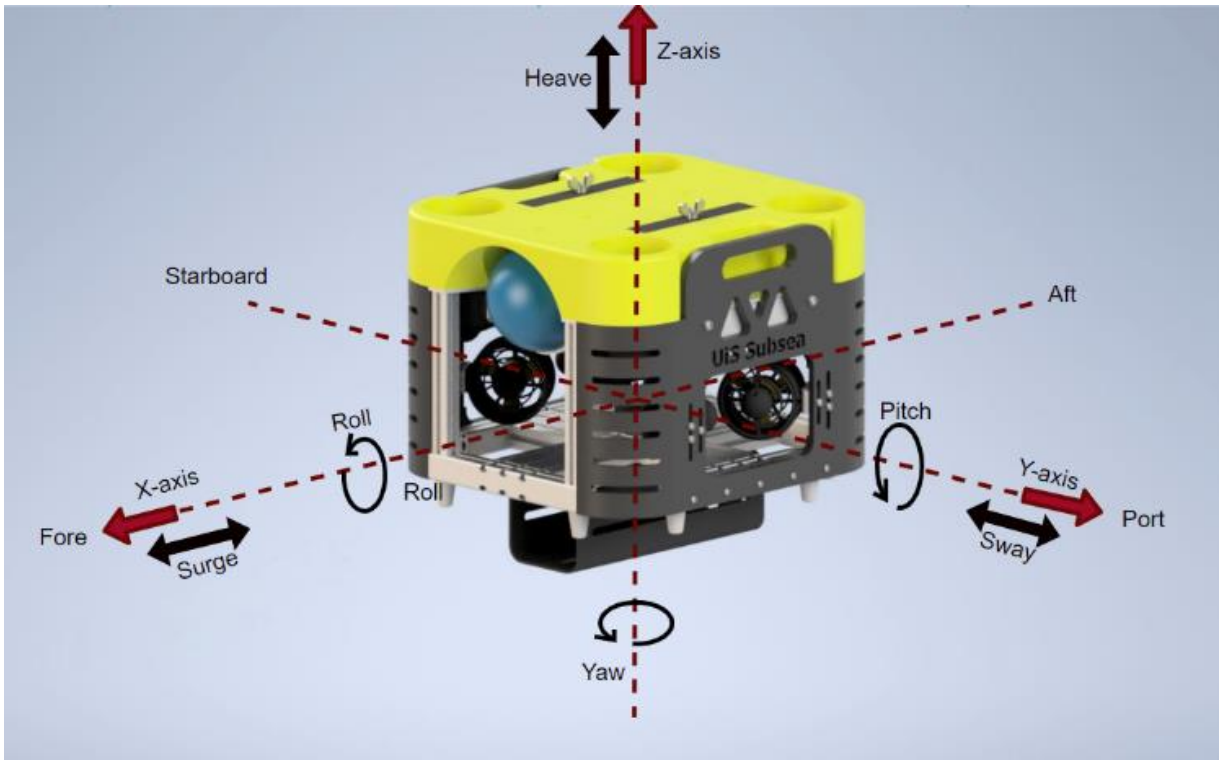

Figure 2 ROV orientation and movement

Manipulator

A ROV may need to perform tasks while operating. Therefore, most ROVs are equipped with a manipulator. The manipulator is explained in the quote below.

> *"A robot manipulator is an electronically controlled mechanism, consisting of multiple segments, that performs tasks by interacting with its environment. They are also commonly referred to as robotic arms."* [5]

Most manipulators will resemble the human arms because they have become extremely flexible and can perform almost any task. Designing a manipulator is easier when one is familiar with how an arm operates and how it would reach for a given object.

DOF (Degrees of Freedom)

DOF is a number for how many rotational joints there are in a manipulator arm. In Figure 3, examples of one, three and six DOF using only revolute joints are shown. Where θ is the joint angle and provides one DOF for each new θ.

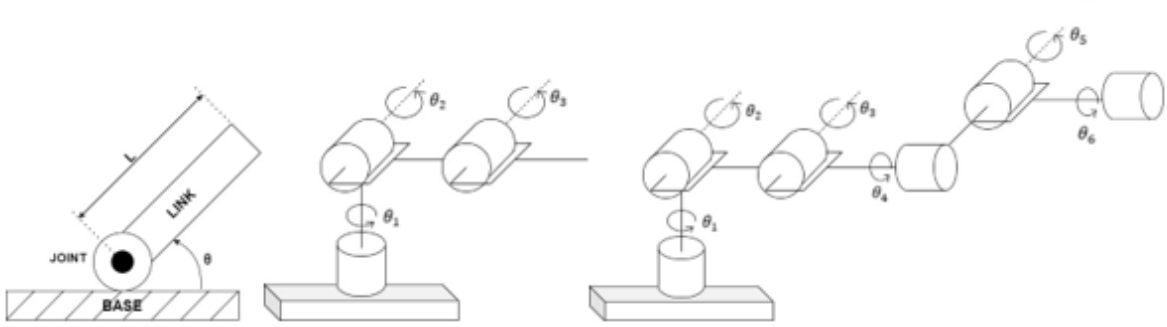

Figure 3 One, three and six DOF

Manipulators may also be built using prismatic joints or spherical joints. The prismatic joints provide linear motion along one axis. Spherical joints are the same as a human shoulder, providing motion in the 3D space.

End effector

Often called the gripper or hand of a robot manipulator. An end effector may be more than this. A needle for sewing patients or a suction cup for lifting boxes, both are end effectors. A short explanation follows below.

> *"An end effector is a peripheral device that attaches to a robot's wrist, allowing the robot to interact with its task. Most end effectors are mechanical or electromechanical and serve as grippers, process tools, or sensors. They range from simple two-fingered grippers for pick-and-place tasks to complex sensor systems for robotic inspection."* [6]

In subsea operations most ROVs use a gripper. Usually having between two and five fingers. This allows for the completion of most tasks such as, cutting wires, installing new equipment or removal of debris. Having a versatile end effector has the benefit of spending less time at the surface and more time performing work.

1.3 Subsea Industry

The subsea firms in Norway and especially within the Stavanger region are world leading within their field. The firms in Norway mostly operates in the Oil and Gas industry, but the operations are increasing in other fields such as, mineral exploration, salmon farms, renewable energy, and outer space. For several decades to come, the Norwegian continental shelf and in other countries territorial waters as well, decommissioned subsea installations must be removed, and ROVs are great at such jobs.

To overcome the challenges within these industries a broad range of ROVs have been developed. Some examples are AUVs (Autonomous Underwater Vehicles), observation ROVs and work class ROVs. AUVs are usually not equipped with a manipulator and is therefore irrelevant for this project. Work class ROVs are usually equipped with two arms. One which usually just holds onto a grab point such that the other more precise arm can do the work. An observation ROV may or may not be equipped with one manipulator. A study of the existing solutions is necessary to gain an understanding in the design of these.

Below are two examples from the Oceaneering website [7].

1. Heavy work class ROV Magnum ® Plus ROV, shown in Figure 4. The ROV is run on hydraulics and the total weight is 3060kg. Equipped with two manipulators. The left manipulator is used for holding onto a grab point while the right arm performs precision work. To be able to perform heavy duty work, hydraulics is still the better choice for the harsh conditions this ROV operates in.

Figure 4 Oceaneering's Heavy work class ROV Magnum ® Plus ROV

2. Observation and inspection ROV Omni Maxx ROV, shown in Figure 5. The only full electrically powered ROV from Oceaneering. At a weight of 270 kg, it is the lightest standalone ROV in Oceaneering's assets. The ROV is equipped with one manipulator. Because this ROV is mostly used for observation and inspection, there is no need for a powerful manipulator. Instead, it is designed to be small, light weighted and agile.

Figure 5 Oceaneering's Observation and inspection ROV Omni Maxx ROV

This indicates that using electrical power for controls, at least of the manipulator is uncommon in the industry. Reasons for using hydraulic may be that most electrical equipment must release heat in a way that hydraulics does not. Therefore, cooling systems are necessary which will increase the overall ROV weight. The electrical wires cannot get in contact with water. It is possible to keep the electrical motors in a waterproof box, but the shaft is usually in contact with water and it is nearly impossible to keep rotating equipment totally waterproof. Hydraulics is a solid system which is proven to work in harsh condition and provides great power, while requiring a small amount of space.

1.4 MATE

In the MATE competition it is possible to score a maximum of 675 points where most points are from performing the tasks (270 points), engineering presentation (100 points) and technical documentation (100 points). The focus of UiS Subsea will be to get the highest score possible within these three above categories.

For detailed information, see the MATE EXPLORER manual [4], MATE mission video [8] and Appendix A.

The manipulator must be a manifestation of the information in Appendix A and should be able to perform all if not most tasks. Most importantly, the manipulator should not be the reason for disqualification. Participants are also encouraged to act professionally, and every action performed must be done in a safe manner. Therefore, MATE will not hesitate to disqualify companies that do not meet the safety standards.

Going through all the information regarding the competition is a time-consuming job and UiS Subsea has spent several weeks identifying, planning and summarizing objectives. This made it easier for each individual team member to know their role in the project.

In short, the requirements to not disqualify

- Follow safety procedures
- Meet deadlines
- Waterproofed electrical equipment must withstand a depth of at least 7 m
- ROV weight must be less than 35 kg
- ROV size must be within a 92 cm diameter sphere

Other requirements for the completion of the given tasks

- Grab a 60 mm OD (outer diameter) pipe
- Grab a 21 mm OD pipe
- Hold a small rope
- Lift 5 N
- Pick up a zip-lock bag
- Pull out a 5 mm pin

1.5 Previous work

UiS Subsea has been participating in MATE since 2013 and there are ROVs and manipulators from these years available. Unfortunately, some of the previous work have been lost and some ROVs are missing their manipulators. The only manipulator that was found to be still in good shape is the one from 2015. This manipulator was the work of 7 people split into 4 theses.

Electrical

"Beregning og styring av manipulator for fjernstyrt undervannsfarkost" [9]

Design

"Produktutvikling av elektrisk manipulator til ROV" [10]

Analysing

"Design, kinematic analysis and (multibody) simulation of manipulator mechanism for underwater robot (using ADAMS) " [11]

End effector

"Product development and testing of tools for ROV" [12]

The manipulator from 2015 is a fully electric manipulator powered by 6 stepper motors. Two motors work in a pair to drive the first link. Two work in a pair to create rotation and tilt of the end effector. One drives the second link and one for the grip mechanism. The motors transmit power through belts to create rotation of the joints and a steel wire to create the grip motion. The high numbers of motors contribute to a high overall weight and the placement of the motors make the manipulator wide, taking a lot of space.

Figure 6 is a picture taken in 2021 of the 2015 manipulator with 4 of the motors removed.

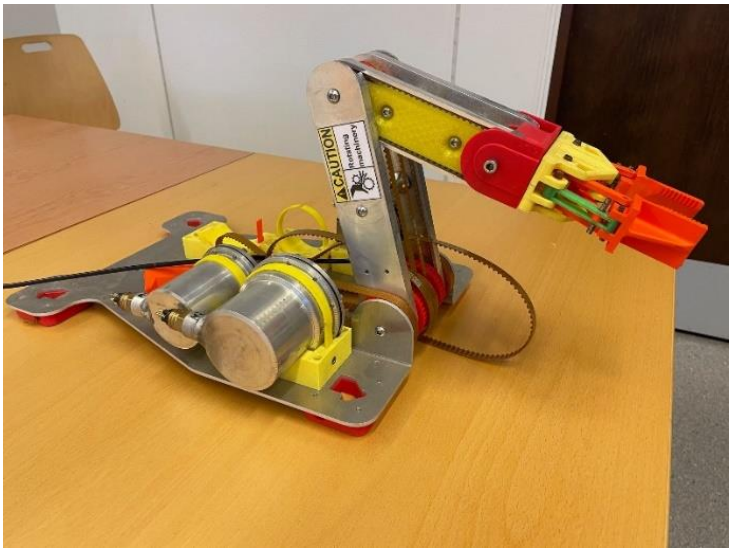

Figure 6 Manipulator 2015

Figure 7 shows the motor setup of the 2015 manipulator.

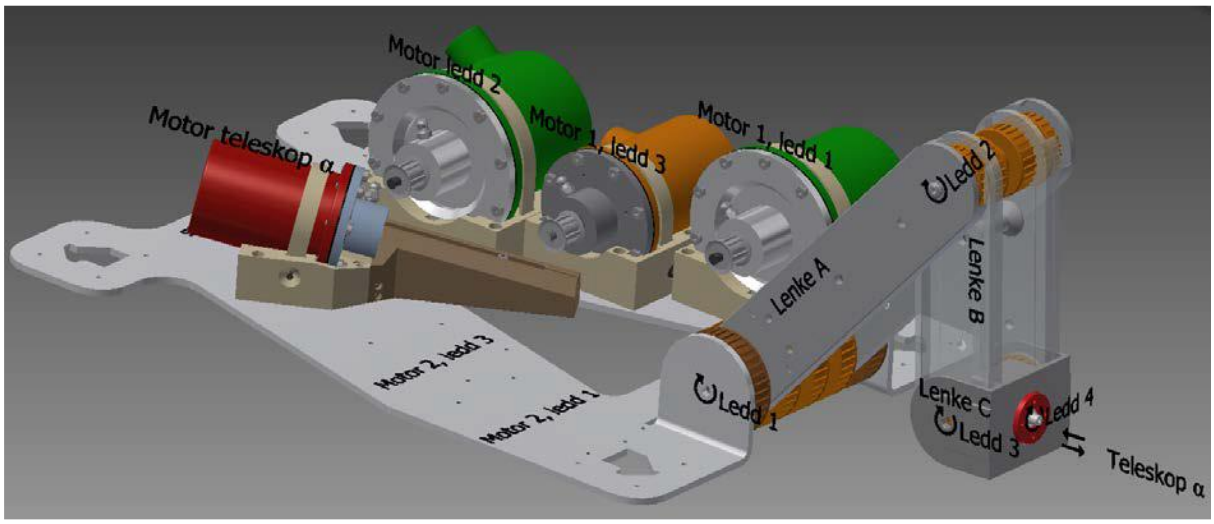

Figure 7 Motor setup 2015 [10, p. 15]

The workspace for this manipulator is shown in Figure 8.

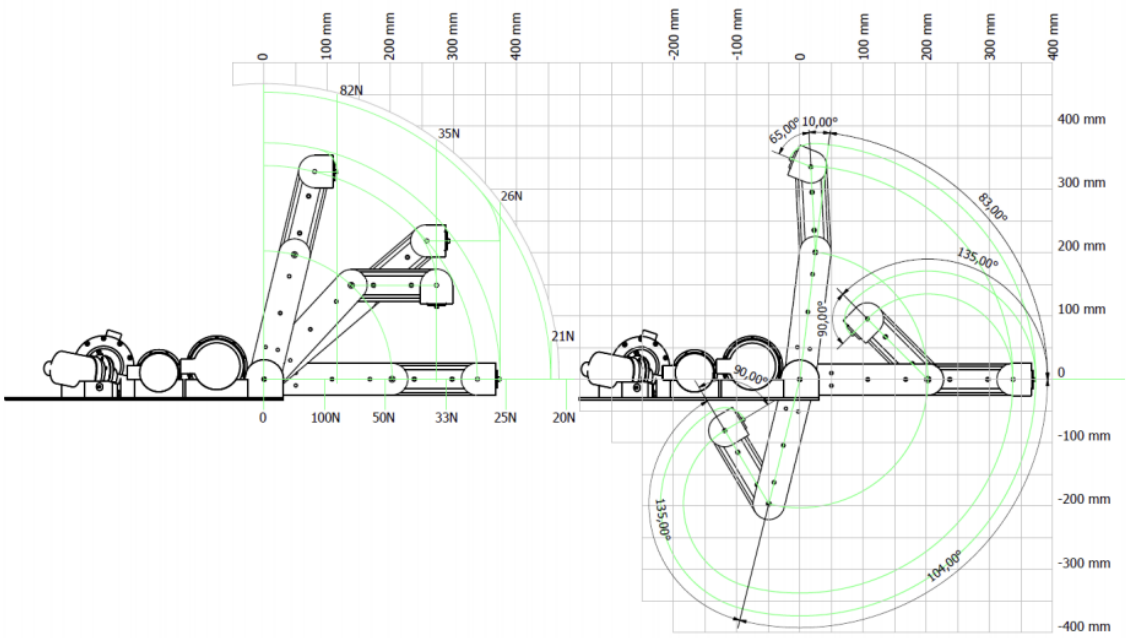

Figure 8 Manipulator workspace 2015 [10, p. 30]

Some of the other specifications for the 2015 manipulator

- Three Nema 24 stepper motors
- Two Nema 17 stepper motors
- One Nema 14 stepper motor
- 4 DOF
- Weight 8802 g

This manipulator would easily be able to lift 5 N for this competition, but it is far too heavy, and its size is not compatible with the overall ROV design of this year. There is clearly a lot of potential to reduce weight and size. It should not be necessary to use two motors for each link. The use of belts adds no holding torque and therefore the arm relies on the holding torque of the motors to stay in position. The overall design is good and the differential gearing to achieve the tilt and rotation of the end effector is a great solution, but the manipulator is not suited for this year's competition.

1.6 Limitations and contribution

Designing and building an industrial manipulator is a process that usually takes years and has a high cost. Hobby manipulators are available at low costs and most information needed to design one is already out there. This project will require smart solutions and must reduce time consumed where possible.

It is a big project and not every topic will be covered, and the project has some limitations which are shown below

- The project is set to last for 5 months
- The budget is limited to 7000 NOK
- Little prior knowledge of subject

Participating in this competition promotes learning and teamwork in a way that a regular project would not. UiS Subsea is responsible for passing on the project to students for the next year and to promote subsea studies.

Contribution this year will be

- A functional electric driven manipulator
- Gripper as the end effector
- Motion simulation in Adams
- Engage other students in robotics and subsea applications

To achieve this, some goals had to be set. Good goals are quantifiable and can be measured for improvement in the future. This led to the following goals

- To be among the top 10 contestants in MATE ROV Competition
- A functional, modular ROV manipulator for use on land and in water
- Do not exceed the budget of NOK 7000 for the manipulator
- Reduce weight compared to the 2015 manipulator by 40%

2. Theory

This chapter will focus on the relevant theory within the manipulator such as its parts, mechanisms, and motion. The project will not delve deep into each field but will instead provide a framework for future work.

The links for the manipulator in this project is assumed to be rigid and will have no deflection, this will simplify calculations. This is possible due to the low speed and loads. For a real application which requires higher accuracy and speed, this simplification will not be valid.

2.1 Robot arm configurations

Robotic arms are being used as a replacement of the human hand and will be able to execute different tasks without taking any risks when it comes to human lives. The efficiency can be far greater compared to human labour as they can be programmed to do quick movements with high precision.

Robotic arms are split into the 6 categories below [13].

1. **Polar coordinate robot**

A robotic arm placed on a rotating platform with an extendable arm which can tilt up or down. This robotic arm relies on the polar coordinate system, hence the name. A polar coordinate robot is illustrated in Figure 9.

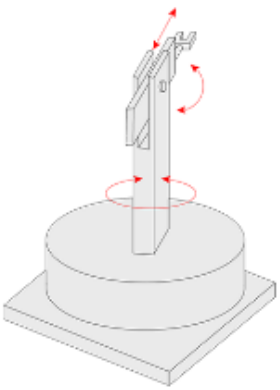

Figure 9 Polar coordinate robot [13]

2. Cylindrical coordinate robot

Very similar to the polar coordinate type but instead of a revolute joint causing the vertical movement, it uses a prismatic joint for the vertical movement. It is built to resemble the cylindrical coordinate system. Illustrated in Figure 10.

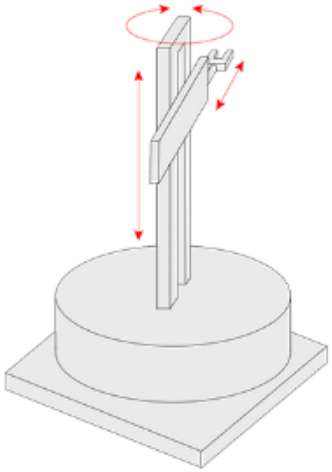

Figure 10 Cylindrical coordinate robot [13]

3. Cartesian coordinate robot

This arm can move horizontally, vertically and can extend the arm. It cannot rotate, and will always be perpendicular to each axis. This robotic arm uses the coordinate system XYZ and is therefore easy to configure. Illustrated in Figure 11.

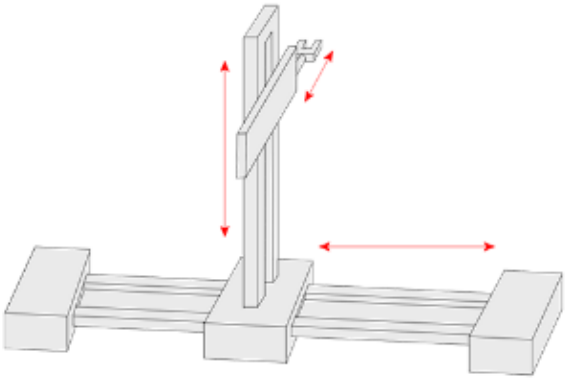

Figure 11 Cartesian coordinate robot [13]

4. Articulated robot

This arm resembles the human arm, with parts that can be associated with shoulder, arm, and wrist. It is one of the most common type of robotic arm in the industry because of its versatility. An illustration of an articulated robot is given in Figure 12.

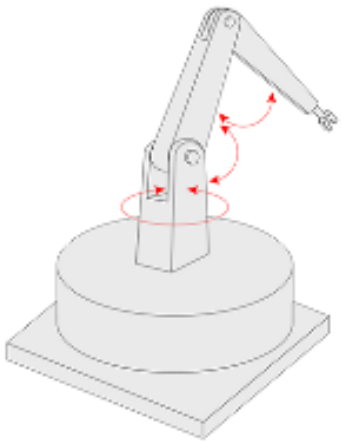

Figure 12 Articulated robot [13]

5. SCARA (Selective compliance assembly robot)

Known as the assembler. This robotic arm is mostly used in operations with flat surfaces such as assembling circuit boards. It is widely used in pick and place processes that requires the arm to do fast repetitive tasks. The arm is limited to horizontal movement, but the effector can be raised and lowered. SCARA robot configuration is illustrated in Figure 13.

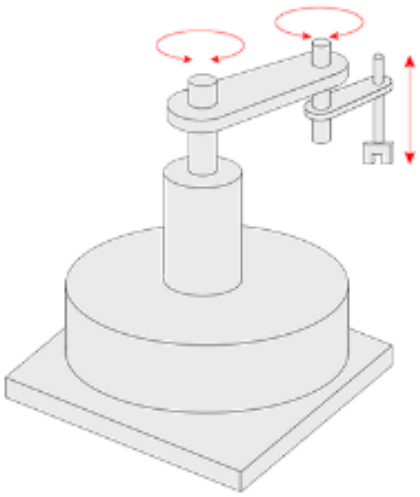

Figure 13 SCARA robot [13]

6. Parallel link robot

More commonly referred to as a delta robot. Three arms control the effector, and thus is very limited, but it can move fast at the cost of movement range. It is mainly used in sorting tasks, such as food or smaller parts moving on a conveyor belt. A parallel link robot is illustrated in Figure 14.

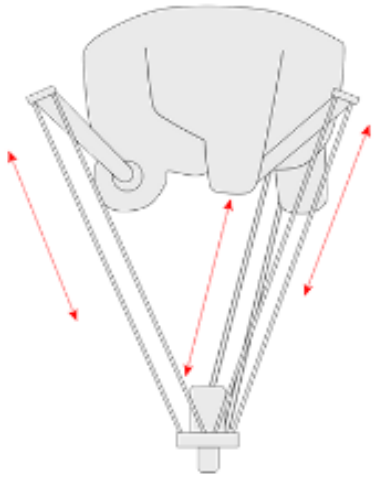

Figure 14 Parallel link robot [13]

Of these different types, the articulated robotic arm is the one that is most suitable for a ROV. This is due to it being suited for most applications, whereas most other configurations are for repetitive special cases.

2.2 Kinematics

Kinematics studies the motion of the object and do not consider masses or forces. Where the motion is position, velocity, and acceleration of the object. For accurate controls of moving parts, kinematic studies are a must.

In robotics kinematics is used to describe the position of the robot at any given moment. Having the position of each of the manipulator's links and end effector is crucial for the operation. Within robotic kinematics there are two different branches that solve the same problem using different methods. The methods described here is adapted from [14, pp. 233-371].

2.2.1 Forward Kinematics

Forward simply means going from the base of the manipulator forward to the end effector. The position of each joint is known with their respective angles and the objective is to find the position of the end effector in terms of coordinates x, y, z.

The easiest way to calculate the forward kinematics for a low DOF manipulator is to use the geometric approach. A planar two DOF manipulator is illustrated in Figure 15.

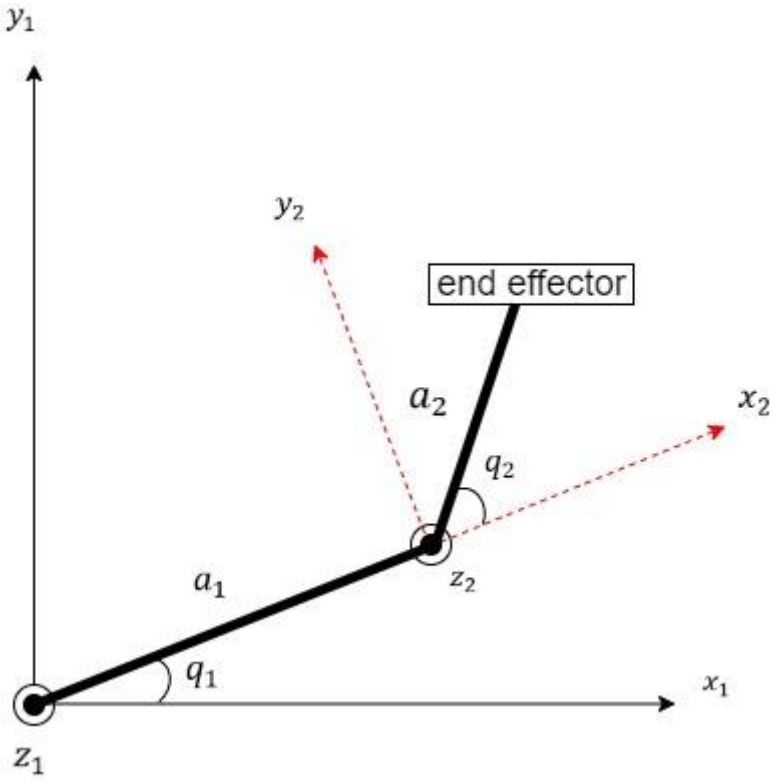

Figure 15 Two DOF planar manipulator

The solution as a position vector is

$$\vec{p} = \begin{pmatrix} x \\ y \end{pmatrix} = \begin{pmatrix} a_1 \cos q_1 + a_2 \cos(q_1 + q_2) \\ a_1 \sin q_1 + a_2 \sin(q_1 + q_2) \end{pmatrix} \quad (1)$$

The general approach is to determine the DH (Denavit-Hartenberg) parameters for each link and use matrix multiplication for each of these matrices to get the result.

The 4 parameters are as follows [15]

l_i – Displacement along the previous joint's z-axis

q_i – Rotation about the previous joint's z- axis

a_i – Displacement from previous z-axis along the current joint's axis

β_i – Rotation about the current joint's x-axis

Where i is the link number, starting from 0 at the base.

The DH transformation matrix is

$$\mathbf{{}^{0}_{i}T} = \mathbf{{}^{i-1}_{i}T} \tag{2}$$

where

$$\mathbf{{}^{i-1}_{i}T} = \begin{pmatrix} cosq_i & -sinq_i cos\beta_i & sinq_i sin\beta_i & a_i cosq_i \\ sinq_i & cosq_i cos\beta_i & -cosq_i sin\beta_i & a_i sinq_i \\ 0 & sin\beta_i & cos\beta_i & l_i \\ 0 & 0 & 0 & 1 \end{pmatrix} \tag{3}$$

and is equal to

$$\mathbf{{}^{i-1}_{i}T} = \begin{pmatrix} & & & x \\ & \boldsymbol{R} & & y \\ & & & z \\ 0 & 0 & 0 & 1 \end{pmatrix} \tag{4}$$

where ***R* is** a 3x3 DH rotation matrix for the transformation. After computing the transformation matrix, simply read off the coordinates x, y, and z in the last column of the transformation matrix.

Example for the two DOF planar manipulator, where the DH parameters are shown in Table 1.

Table 1 DH parameters two DOF planar manipulator

Link	a_i	β_i	l_i	q_i
1	a_1	0	0	q_1
2	a_2	0	0	q_2

For the first link Eq. (3) gives

$$ {}^{0}_{1}\boldsymbol{T} = \begin{pmatrix} cosq_1 & -sinq_1 & 0 & a_1 cosq_1 \\ sinq_1 & cosq_1 & 0 & a_1 sinq_1 \\ 0 & 0 & 1 & 0 \\ 0 & 0 & 0 & 1 \end{pmatrix} \tag{5} $$

and for the second link Eq. (3) gives

$$ {}^{1}_{2}\boldsymbol{T} = \begin{pmatrix} cosq_1 & -sinq_1 & 0 & a_1 cosq_1 \\ sinq_1 & cosq_1 & 0 & a_1 sinq_1 \\ 0 & 0 & 1 & 0 \\ 0 & 0 & 0 & 1 \end{pmatrix} \tag{6} $$

multiplying Eq. (5) and Eq. (6) results in

$$ {}^{0}_{2}\boldsymbol{T} = \begin{pmatrix} cos(q_1 + q_2) & -cos(q_1 + q_2) & 0 & a_1 \, cos \, q_1 + a_2 \, cos(q_1 + q_2) \\ cos(q_1 + q_2) & cos(q_1 + q_2) & 0 & a_1 \, sin \, q_1 + a_2 \, sin(q_1 + q_2) \\ 0 & 0 & 1 & 1 \\ 0 & 0 & 0 & 1 \end{pmatrix} \tag{7} $$

the first two rows in the last column is now the (x, y) coordinates for the two DOF planar manipulator. This is the same solution as using the geometric approach. Now let q_i and l_i be functions of time, then the position vector is given as

$$ \vec{p}(t) = \begin{pmatrix} x(t) \\ y(t) \end{pmatrix} \tag{8} $$

the velocity vector is found by differentiating Eq. (8)

$$ \vec{v}(t) = \frac{d\vec{p}(t)}{dt} \tag{9} $$

and the acceleration vector is found by differentiating Eq. (9)

$$ \vec{a}(t) = \frac{d\vec{v}(t)}{dt} = \frac{d^2\vec{p}(t)}{dt^2} \tag{10} $$

If the manipulator consists of only revolute joints, then l_i will be constant over time and the calculations will simplify. This is the case for the two DOF planar manipulator.

2.2.2 Inverse Kinematics

Inverse is the opposite of forward, where one goes from the end effector towards the base. The position of the end effector is given, and the objective is to find the angle of each joint when in this position. Inverse kinematics is harder to solve than forward kinematics due to the non-linear number of solutions. There is no general approach to solving these equations. Instead there are multiple ways to calculate these and it is normally handled by computers using an analytical or numerical approach.

This project will only deal with the inverse kinematics problem for a two DOF manipulator. A two DOF planar manipulator has two different solutions as shown in Figure 16.

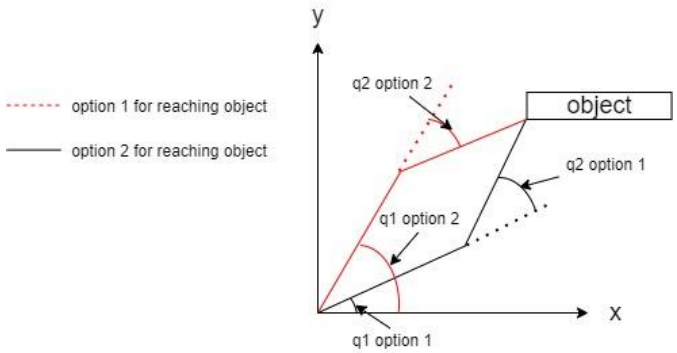

Figure 16 Two solutions for reaching an object

The forward kinematic solution is given by Eq. (1), and by solving for the second joint angle one will find that

$$q_2 = \pm 2\tan^{-1}\sqrt{\frac{(a_1+a_2)^2-(x^2+y^2)}{(x^2+y^2)-(a_1-a_2)^2}} \tag{11}$$

where the ± indicates two solutions, in this case these solutions are called elbow up or elbow down. In Figure 16, option 1 is elbow up and option 2 is elbow down.

The first joint angle is

$$q_1 = \tan^{-1}\frac{y}{x} \pm \tan^{-1}\frac{a_2 sinq_2}{a_1 + a_2 cosq_2} \tag{12}$$

Note that the first joint angle is dependent upon the second joint angle.

2.3 Angled gripper

An angled gripper functions by having a force exerted on a type of fingers to hold an object. In Figure 17 this type of function is achieved by having a downward applied force, $F_{applied}$, which is split evenly between the fingers by the angle φ.

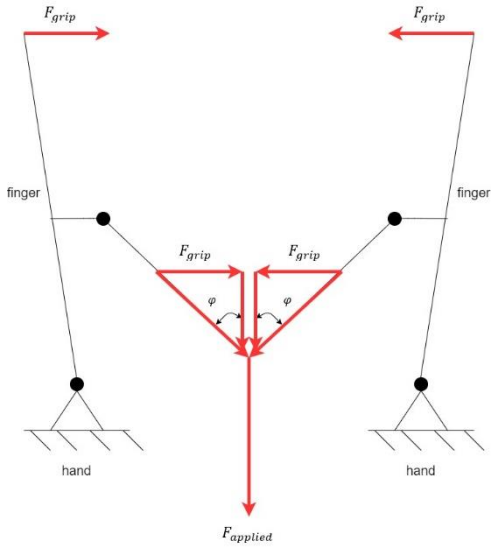

Figure 17 Angled gripper

The resulting grip force is then

$$F_{grip} = \frac{F_{applied}}{2} \tan \varphi \tag{13}$$

By inspection, should the angle φ increase, the grip force will increase. However, it is not possible to achieve the maximum force, because $\tan \varphi$ diverges towards infinity when φ closes in on 90º. There are also mechanical limitations in place, which will prevent the extreme angles from occurring.

2.4 Mechanical and electrical components

This chapter presents relevant components and the respective theory needed for this manipulator. Achieving all the desired functions of a manipulator requires extensive knowledge within mechanical and electrical components. There are almost an infinite number of ways to connect joints and creating movement which makes choosing a set of components a time-consuming process.

2.4.1 Belts

Belts are used for transmission between shafts that are far apart. An alternative to belts may be chains which provides higher strength at the cost of more weight and cost. Other alternatives where the centre distance is small may be gears. Unlike gears, belts will provide the same rotation in the same direction for both shafts.

Belts are common as they are cheap and requires low precision compared to the alternatives. Most belts are made of a rubber like material that is strengthened by steel cords giving the belt room for elongation. This is in turn may require some option for tightening the belt, as it tends to increase its length over time. Equipment that operates at low speeds may not need tightening mechanisms. If there are no tightening mechanism, then it is important to install the pulleys at the correct centre distance to maintain the tension in the belt. Figure 18 shows an example of a belt transmission setup.

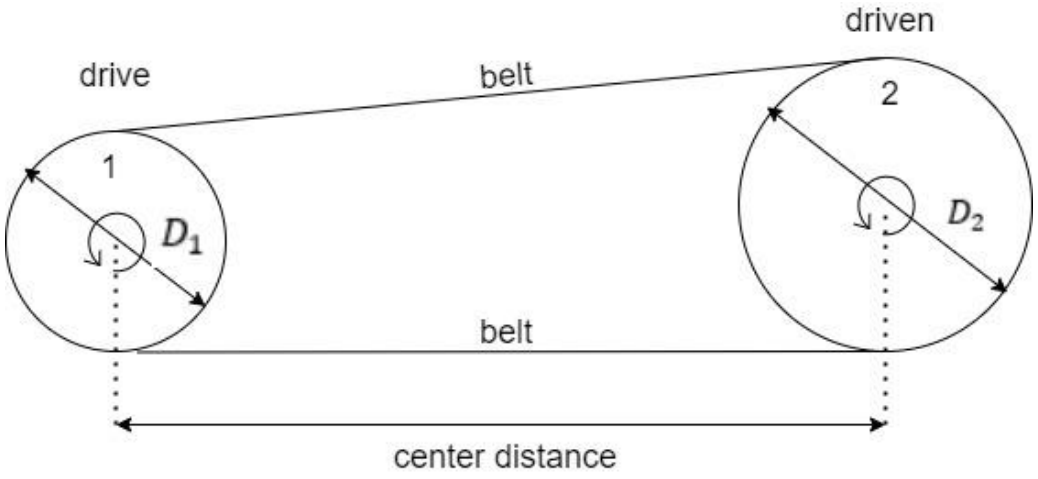

Figure 18 Belt transmission

Effect factor for torque transmitted by the belt may be written as

$$i_{transmit} = \frac{D_2}{D_1} = \frac{n_1}{n_2} \tag{14}$$

where n_i is the RPM of the pulley and D_i is the pulley diameter.

2.4.2 Springs

Springs are widely used in mechanical structures as they are unique in storing mechanical energy and can return to their former positions given no deformations. Springs work either by compressing or by extension and calculations will be the same for both types. Springs connected in parallel will have their spring constants k_i, be added into one equal spring constant as shown in Figure 19.

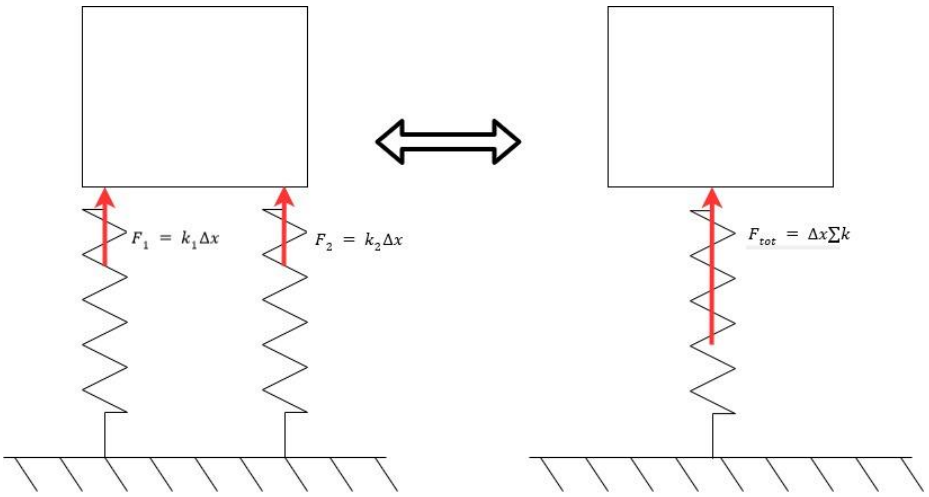

Figure 19 Springs in parallel

The extension or compression force is simply

$$F_{tot} = \Delta x \sum k \tag{15}$$

where Δx is the change in length of the springs.

2.4.3 Ball bearings

Ball bearings are used in almost all rotating equipment because it reduces friction between a rotating part and its mated part. It can used on a shaft to create parts which rotates independently of each other. The ball bearing uses balls to create the rolling motion and has a point of contact between the ring and balls. This enables it to accommodate both radial and axial load without the need of other configurations.

Factors for decision of a ball bearing may include, but not limited to

- Price
- Loads
- Environment
- Rotational speed
- Lifetime
- Dimension
- Availability

In small robotics most bearings accommodate small loads and because of this not much effort besides price, dimension and availability has been considered. For more info on how to select correct bearing for an application, SKF webpage is recommended [16].

2.4.4 Screws, bolts, nuts

Clarifying the difference between a bolt and screw. A bolt requires a threaded or wide enough hole to go through with its threaded part and then be tightened with a nut. A screw is self-penetrating and requires either no hole or a hole small enough for its threaded part to eat into the material.

Screws are primarily used in soft materials, such as wood, plastic, or thin metal plates. As a screw is self-penetrating the screw should not be removed once installed. The hole widens and the strength loss is considerable.

Bolts are used in all construction materials as one can either, make a hole wide enough or thread the mating part. The use of bolts is one of the dominant and most user-friendly fastening methods, making it possible to remove and install a part repeatedly.

Seeing as the loads to be accommodated are small and the risk of high vibrations is minimal, there should be no risk for the different fastening components to fail. Instead the focus will be to not overtighten the screws and bolt.

2.4.5 Worm gear pair

Using worm and worm gear allows for a much greater holding torque for the motors. This is due to the large normal force between the gears, resulting in a large frictional force which locks the pair in place. This is especially useful for motors with a low holding torque. Worm gears are also useful due to the possibility of high gear ratios compared to normal gears. A 1:60 ratio between a worm and a gear would mean 60 full revolutions of the worm to turn the gear one revolution.

All calculations in this project will follow the examples from KHK Gears [16]. Figure 20 gives an overview of the forces in a worm gear pair. While Figure 21 (a) shows the decomposed forces acting on the worm and Figure 21 (b) shows the frictional components of the force.

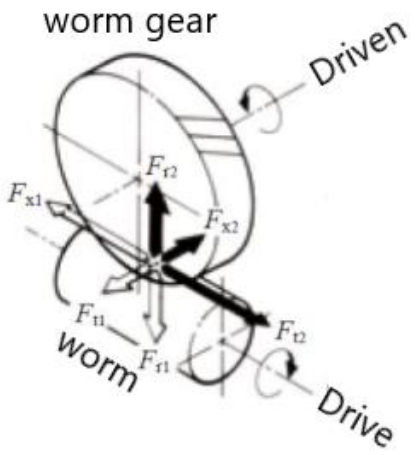

Figure 20 Forces in a worm gear pair [16]

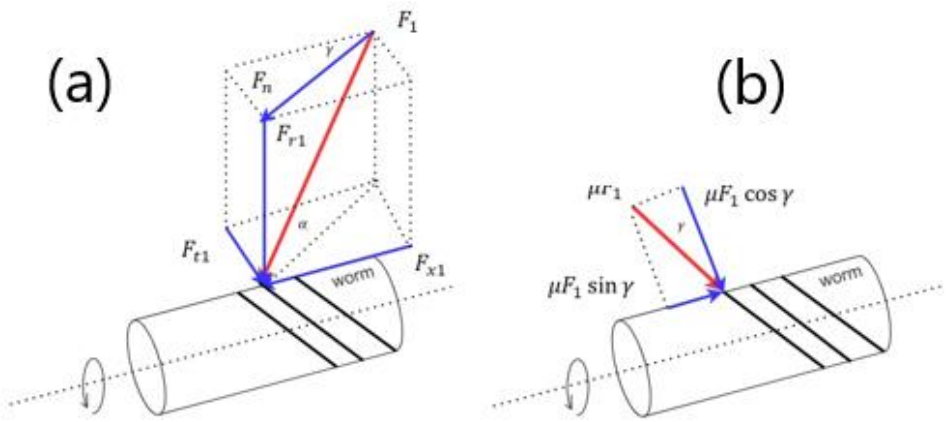

Figure 21 (a) Forces acting on worm (b) Frictional components of force acting on the worm

This project will only consider an angle of 90º between the worm and the worm gear, which will give the relations below.

Axial component of the worm is equal to the tangential component of the worm gear

$$F_{x1} = F_{t2} \tag{16}$$

Tangential component of the worm is equal to the axial component of the worm gear

$$F_{t1} = F_{x2} \tag{17}$$

Radial component of the worm is equal to the axial component of the worm gear

$$F_{r1} = F_{r2} \tag{18}$$

The condition for a self-locking worm pair is when the static friction is higher than the tangent of the lead angle of the worm

$$\mu_s \geq tan\,\gamma \tag{19}$$

and the lead angle of the worm is

$$\gamma = \tan^{-1}\left(\frac{mz_1}{d_1}\right) \tag{20}$$

where

$m - Module$

$z_1 - Number\ of\ teeth\ on\ the\ worm$

$d_1 - Worm\ diameter$

Efficiency of the worm gear pair may be written as

$$\eta = \frac{tan\gamma F_{t2}}{F_{t1}} \tag{21}$$

The tangential component of the worm gear is

$$F_{t2} = F_{t1}\frac{cos\,\alpha\ cos\,\gamma - \mu\, sin\,\gamma}{cos\,\alpha\ sin\,\gamma + \mu\, cos\,\gamma} \tag{22}$$

Where α is the reference angle, usually 20°. The tangential component of the worm is

$$F_{t1} = \frac{2T_{in}}{d_1} \tag{23}$$

Output torque is given as

$$T_{out} = \frac{F_{t2}d_2}{2} \tag{24}$$

where

$d_2 - Worm\ gear\ diameter$

T_{in} & T_{out} are given in Nmm and d_1 & d_2 are given in mm

2.4.6 Press fits

Press fits may be used where other means of fastening are deemed unnecessary or not possible. Bearings, shafts and sealings are all components which can use press fits. Often a press fit is the last resort, as it requires extreme precision and the production is time consuming. The project will use methods described in [17, pp. 191-198]

Graphical explanation of terms used are given in Figure 22 and Figure 23.

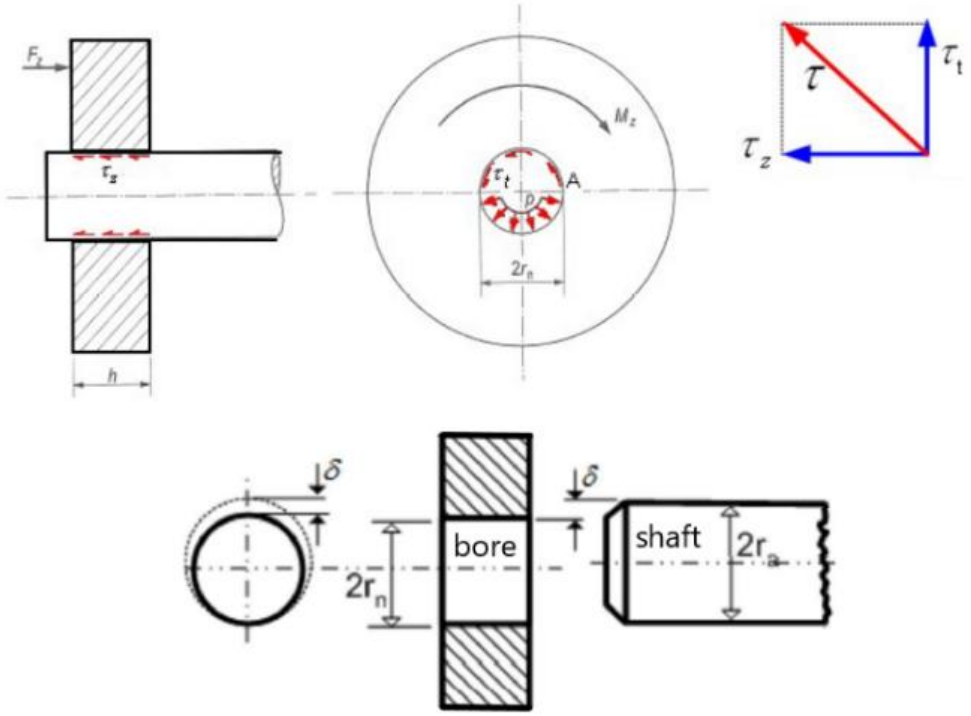

Figure 22 Press fit terms 1/2 [17, p. 191]

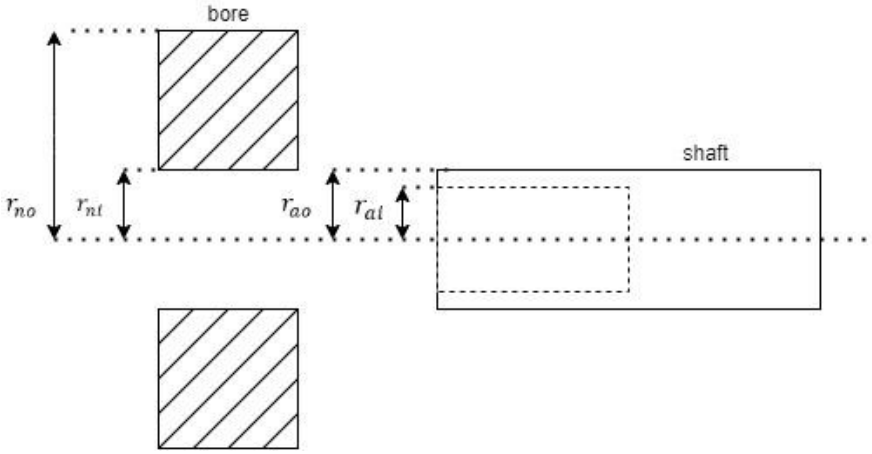

Figure 23 Press fit terms 2/2

The no slip condition for press fits is found by comparing the magnitude of shear stress against the contact pressure multiplied by the coefficient of friction

$$\tau \leq p\mu \tag{25}$$

where μ is the coefficient of friction.

The shear stress magnitude is

$$\tau = \sqrt{\tau_t^2 + \tau_z^2} \tag{26}$$

The tangential shear stress is

$$\tau_t = \frac{M_z}{2\pi r_n^2 h} \tag{27}$$

where

$M_z - Torsional\ torque$

$h - depth\ of\ bore$

$r_n - radius\ of\ bore$

The axial shear stress is

$$\tau_z = \frac{F_z}{2\pi r_n h} \tag{28}$$

where F_z is an axial force. Contact pressure between the shaft and bore may be written as

$$p = \frac{\delta}{2(\alpha_n + \alpha_a)} \tag{29}$$

where

$$\delta = shaft\ diameter - bore\ diameter \tag{30}$$

The bore influence coefficient

$$\alpha_n = \frac{1}{E}\frac{r_{ni}^2}{r_{no}^2 - r_{ni}^2} r_{ni}\left[1 - v + (1+v)\frac{r_{no}^2}{r_{ni}^2}\right] \tag{31}$$

where

$r_{ni} - Inner\ radius\ of\ bore$

$r_{no} - outer\ radius\ of\ bore$

The shaft influence coefficient is

$$\alpha_a = \frac{1}{E}\frac{r_{ao}^2}{r_{ao}^2 - r_{ai}^2} r_{ao}\left[1 - v + (1+v)\frac{r_{ai}^2}{r_{ao}^2}\right] \tag{32}$$

where

$r_{ai} - Inner\ radius\ of\ shaft$
$r_{ao} - outer\ radius\ of\ shaft$

For a solid shaft where $r_{ai} = 0$, Eq. (32) reduces to

$$\alpha_a = \frac{1}{E} r_{ao}(1 - v) \tag{33}$$

2.4.7 Buckling

Buckling may occur in columns that are exposed to a high axial load. Eurocode 3 for stainless steels will be used for calculations in the project. In general, use same approach as for carbon steel, where the only difference is the use of different buckling curves [18, p. 41]. The following steps can be used to find the magnitude of the force which will cause buckling.

1. Determine the effective length factor with the use of Table 2, and multiply it with the measured length to get the effective length

$$L_{cr} = cL \tag{34}$$

where

$c - Effective\ length\ factor$
$L - Measured\ length$

Table 2 Effective length factor [19, p. 9]

Effective length factors. Theoretical values and recommended values when ideal conditions are approximated.						
Buckled shape of column	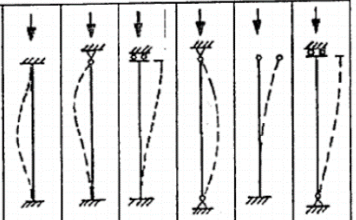					
Theoretical value	0,5	0,7	1,0	1,0	2,0	2,0
Recommended design value	0,6	0,8	1,2	1,0	2,1	2,0

2. Calculate the critical slenderness

$$\lambda_1 = \pi \sqrt{\frac{E}{f_y}} \tag{35}$$

3. Calculate non-dimensional slenderness for a circular solid shaft

$$\bar{\lambda} = \frac{L_{cr}}{D} \frac{4}{\lambda_1} \tag{36}$$

where D is the diameter of the shaft.

4. Find the reduction factor with the use of Figure 24.

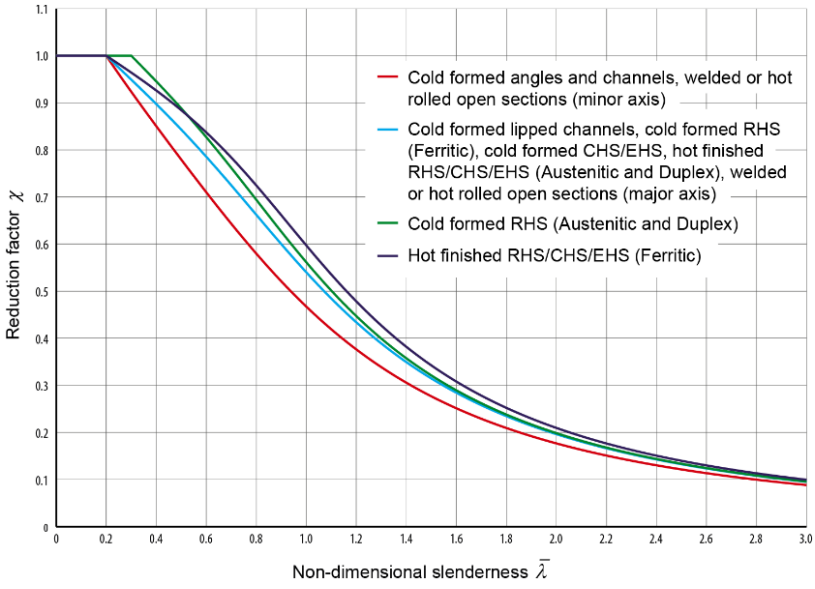

Figure 24; Reduction factor curves for stainless steels [18, p. 65]

5. Calculate critical buckling stress

$$\sigma_{cr} = \chi f_y \tag{37}$$

where χ is the reduction factor.

6. The axial force which will cause buckling

$$F_{allowed} \leq \sigma_{cr} A \tag{38}$$

where A is the cross-sectional area of the shaft

2.4.8 Motors

A ROV manipulator require motors that can be made waterproof, while providing the power and precision needed. The motors presented below are similar. The main difference is a stepper motor use a rotor which is shaped like a gear and is made for precision whereas a BLDC (Brushless Direct Current) has a smooth surface rotor and is optimized for high speeds.

BLDC motor

This motor functions by having magnets in an outer rotor that rotates around the stators in the centre where electric DC (direct current) passes through. It is also possible to have the magnetic rotor in centre, while the stators are in the outer shell of the motor house. BLDC motors are made for constant rotation and therefore has a circular smooth rotor. The motors require little to no maintenance. BLDC motors are widely used in small robotics and provides enough power for most applications.

These motors are easily made waterproof by dipping the coils in epoxy. This is a must in a subsea application and is therefore a perfect fit for use in a manipulator. The downside is that the motor provides low holding torque and will require the correct use of a worm gear to increase it.

Figure 25 shows a BLDC motor where the rotor is placed in the outer shell.

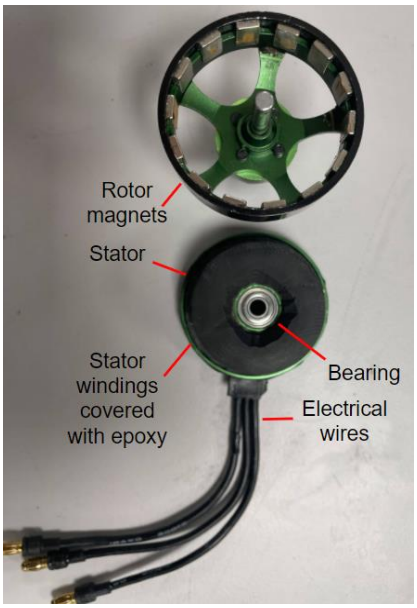

Figure 25 BLDC motor interior

A parameter that hobby BLDC motors have in their datasheet, which can be used to find the RPM (Rotations per minute) of the motor is

$$KV = \frac{RPM}{Voltage} \tag{39}$$

and the RPM is then simply

$$RPM = KV * Voltage \tag{40}$$

Stepper motor

Stepper motors are motors that use pulses for its rotation and are also run on DC. The speed of a stepper motor is measured in PPS (Pulses per second). This motor is made for precise rotation and therefore has a rotor which resembles a gear. The rotor is a permanent magnet and by sending electric pulses through the stators, the stators becomes magnetic and repulses or attracts the rotor. When operating, the motor has a high holding torque which can be further increased by a worm gear pair. See Figure 26 for the different interior components.

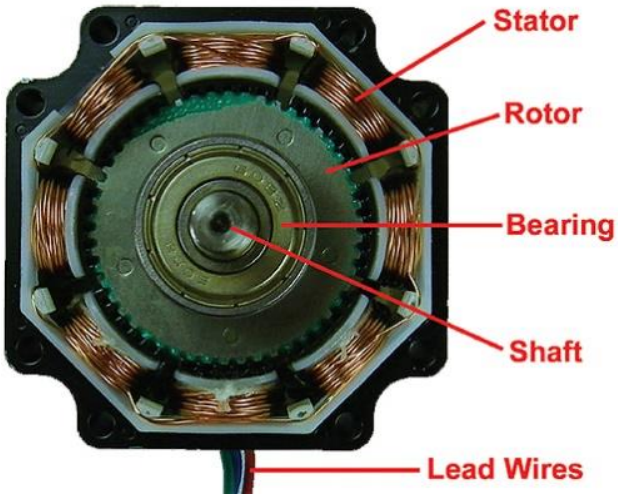

Figure 26 Stepper motor interior [19]

This design allows for great precision and speed control because of the possibility to divide a full rotation into smaller steps. Because of this, stepper motors are often used in different kind of robotics that require great control of motion.

A stepper motor will require an additional housing to become waterproof and the motors produce a lot of heat. A stepper motor will run better at lower speeds due to the on and off switching of the stators, producing resistance which in turn lowers the output torque.

The most relevant specs when choosing a stepper motor is

- Price
- Size and weight
- Pull-out torque
- Holding torque

To find the pull-out torque either perform tests at different speeds or look up in the datasheet for each motor. The latter is the easiest, but there may be some small differences between the datasheet and the motor, and it is recommended to test each motor if there is capacity.

To find the output RPM of a stepper motor, the frequency it should run at is needed. Frequency may be written as [20]

$$frequency = Hz = \frac{step}{second} \tag{41}$$

The motors will run on a stepper motor driver, and it is possible to change the resolution, that is how many steps there is in one revolution, sometimes called micro stepping. The resolution may be written as

$$S = \frac{steps}{rev} \tag{42}$$

Therefore, the RPM for a stepper motor is

$$RPM = \frac{frequency}{S} * 60 \tag{43}$$

It is more intuitive to have the RPM in terms of radians per second, known as angular velocity

$$\omega = RPM * \frac{\pi}{30} = \frac{2\pi * frequency}{S} \tag{44}$$

2.5 Adams

Adams is a MBD (Multibody Dynamics) software and is widely used in simulating designs and concepts. Adams is a powerful tool for simulating motion, vibration, forces, controls, stress, FEA (Finite Element Analysis) and much more [21].

Adams is widely used in robotics because it allows for early evaluation of designs in the development process therefore reducing time spent physically testing the design. This allows a developing company to cut cost and improve the overall design.

Adams goes further than just the kinematics and it is possible to simulate the entire process of the manipulator. Most real-life tasks can be designed and imported into Adams. This makes it a great tool for any engineer working with dynamics in any form. Figure 27 is an example of a

delta configurated pick and place robot where the graphs show the CM (Centre of mass) in x, y, and z direction relative to a given origin.

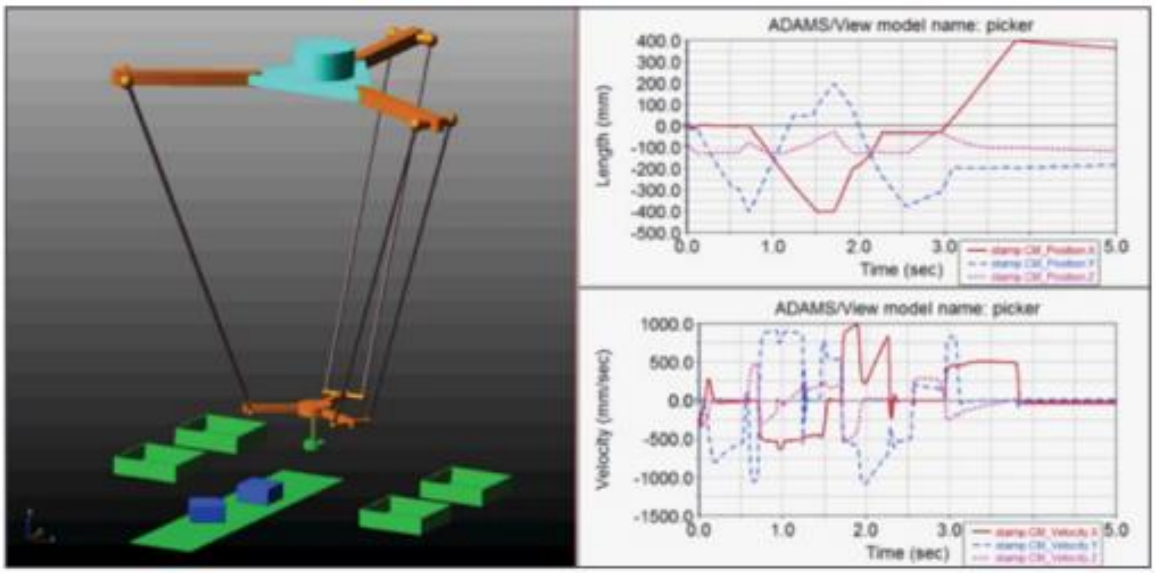

Figure 27; Pick and place simulation in Adams [22]

This project will focus on understanding the kinematics of the manipulator and how Adams can help improve the manipulator. This is done by analysing different parameters such as velocity and acceleration given a specific task. Given enough time, it may be possible to expand into other fields such as controls and stress analysis.

3. Method

For the manipulator to work, a few questions had to be answered. The questions are as follows

- What materials are applicable?
- Is the Nema 17 able to lift 5 N at desired reach?
- What resolution and frequency should the stepper motors run on?
- Are the motors sufficient for use in water?
- How much do the shafts deflect?
- Is the concept working in Adams?

3.1 Materials

The use of correct materials for each component is crucial for the manipulator. The arm is supposed to work on land and submerged in water. Materials must be chosen carefully based on their weight, strengths, and weaknesses. The manipulator will be submerged in fresh chlorinated water at a maximum of 15 minutes, which in turn allows for some slack in the decisions regarding material that corrodes. Three useful material values are

$$E - Young's\ modulus$$
$$f_y - Yield\ strength$$
$$v - Poisson's\ ratio$$

4 materials that are applicable for the manipulator are as follows

1. **PLA (Polylactic acid) for use in 3D printing**

The material resembles oil-based plastic, except that PLA is made of organic material and is therefore biodegradable. The material is used for 3D printing and provides reasonable strength and accuracy at a low cost. It is water resistant and will be slightly negative buoyant in the water. The material is used in 3D printing which makes it possible to increase or decrease the infill. This will change the properties of the finished product. As an example,
Table 3 assumes a 100% infill, so a print of about 80% infill would be slightly positive buoyant in water if there are no leakages for the water to fill the shell.

Table 3 PLA Material properties [23]

Dimensions

Size	Ø tolerance	Roundness
1,75mm	± 0,05mm	≥ 95%
2,85mm	± 0,10mm	≥ 95%

Physical properties

Description	Testmethod	Typical value
Specific gravity	ASTM D1505	1,24 g/cc
MFI	-	6,0 g/10 min
Tensile strength	ASTM D882	110 MPa (MD) 145 MPa (TD)
Elongation at break	ASTM D882	160% (MD) 100% (TD)
Tensile modulus	ASTM D882	3310 MPa (MD) 3860 Mpa (TD)
Impact Strength	-	7,5 KJ/m²

Thermal properties

Description	Testmethod	Typical value
printing temp.	-	180-210˚C
melting temp.	-	210˚C ± 10˚C
melting point	ASTM D3418	145-160˚C
vicat softening temp.	ISO 306	± 60˚C

3D printing will be done using an Ultimaker Cura S5 located at the UiS facilities. A great tool which allows for cheap, fast, and strong parts. It allows for quick prototyping of a component because files can be uploaded directly from a CAD (Computer Aided Design) program onto a USB (Universal Serial Bus). Simply insert the USB in the printer and press play to start the print.

Most parts will be printed with the standard configurations and with the use of breakaway as support material. Parts deemed too weak or where it is necessary to drill holes can be printed with 100% infill. If there is a lower infill than 100% the hole surface will be left with scars from the triangular infill shapes.

2. Aluminium

Aluminium is unique regarding weight to strength ratio and is very resistant to corrosion while being relatively cheap. Aluminium is used in most structures and widely used in marine environments. The material is soft, and machining aluminium compared to steel takes little toll on the equipment. Since aluminium is quite soft, it is not as suited to be threaded as regular steel is.

The stress-strain curves for aluminium are rounded and will use the 0.2% strain rule for deciding yield point, illustrated in Figure 28.

Aluminium material values are assumed to be the averages from MatWeb aluminium alloy [24]

$$E_{alu} = 77{,}4\ GPa$$
$$f_{y,alu} = 278\ MPa$$
$$v_{alu} = 0{,}327$$

3. Stainless steel

Stainless steel is not a specific material but is a term used for a group of steel alloys containing a minimum of 10.5% Chromium. If the steel fulfils the Chromium condition it can be put into one of the 5 following groups of stainless steel types, dependent on their crystalline structure [25]

1. Austenitic
2. Ferritic
3. Martensitic
4. Duplex
5. Precipitation hardening

These 5 classes show little to no corrosion when exposed to humidity over longer periods of time. One of the most common grades, 316, is an austenitic type and is commonly used in the food processing industry.

The stainless steel stress-strain curves are shown to have no clear definition of the yield point and have a curved shape compared to regular steel. That is why the 0.2% strain rule is used for defining the yield point, illustrated in Figure 28.

Stainless steel material values are assumed to be the averages from MatWeb stainless steel [26]

$$E_{stainless} = 196\ GPa$$
$$f_{y,stainless} = 671\ MPa$$
$$v_{stainless} = 0{,}289$$

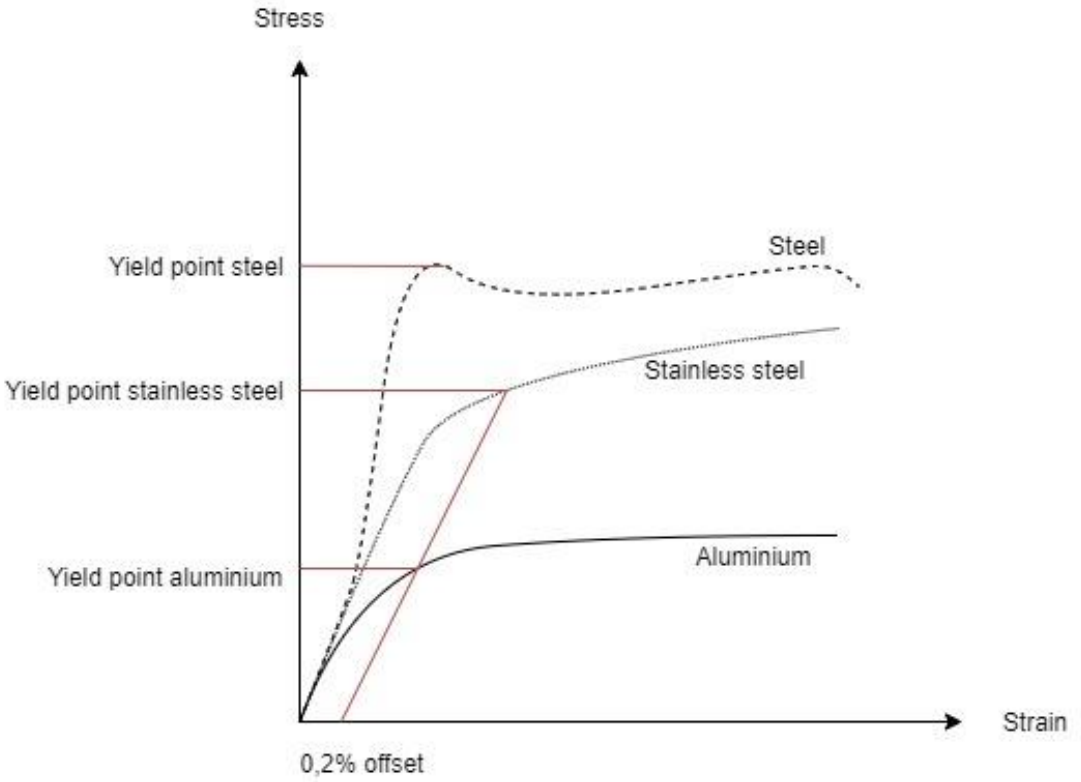

Figure 28 Stress-strain curves

4. Regular steel

The manipulator is to be submerged in water for 15 minutes, making it possible to use regular steel even though it will corrode over time. This project will consider using regular steel bearings if the price of stainless steel bearings exceeds the given budget or if stainless steel bearings are unavailable.

Regular steel the material values are assumed to be the averages from MatWeb medium carbon steel [27]

$$E_{steel} = 203\ GPa$$
$$f_{y,steel} = 685\ MPa$$
$$v_{\ steel} = 0{,}290$$

3.2 Stepper motors

The first test was to gain a better understanding of worm gears and to examine the lifting capacity of a Nema 17 stepper motor. A simple test rig was built as shown in Figure 29.

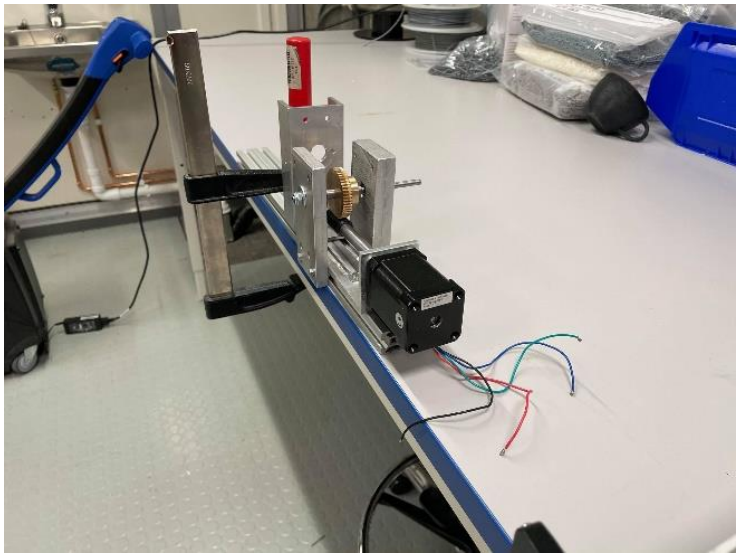

Figure 29 Test rig for lift capacity

The motor should be able to lift 5 N while at maximum reach, 500 mm. Instead of having this reach on the test rig, the length was halved to 250 mm as shown in Figure 30.

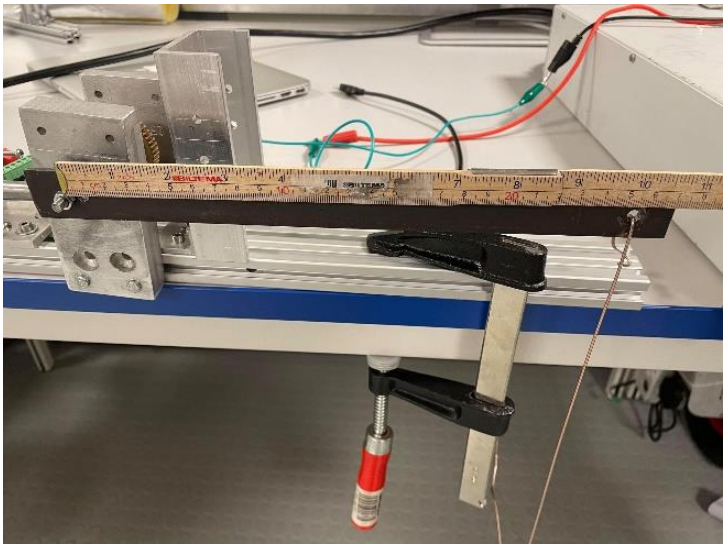

Figure 30 Length of test arm

To achieve the same moment the weight was increased by a factor of two so that it was 10 N. It is assumed that acceleration due to gravity is constant at $g = 9{,}81\ \frac{m}{s^2}$. The motor was to hold and lift a weight of 1774 g, as shown in Figure 31.

Figure 31 Test weight

To decide which resolution the stepper motors should run on, a very simple test consisting of a vice grip and a kitchen weight was made, as shown in Figure 32. Having all other parameters constant and only varying the resolution made it possible to compare which resolution that gave the highest weight. The higher weight the scale read off; the higher torque was provided by the motor.

Figure 32 Stepper resolution test rig

3.3 Waterproof test

To check if the seals in the motor housing were waterproof, the manipulator was submerged in water. It would ideally be submerged to depths like the ones in the competition at 5-10 m, but there were no connectors long enough. Therefore, to test at this depth the ROV needs to be complete and have a long enough tether.

A simple and quick option was to submerge the manipulator in a bathtub, only submerging the motors. The objective of the test was to check the seals and functions while submerged. The test rig is shown in Figure 33.

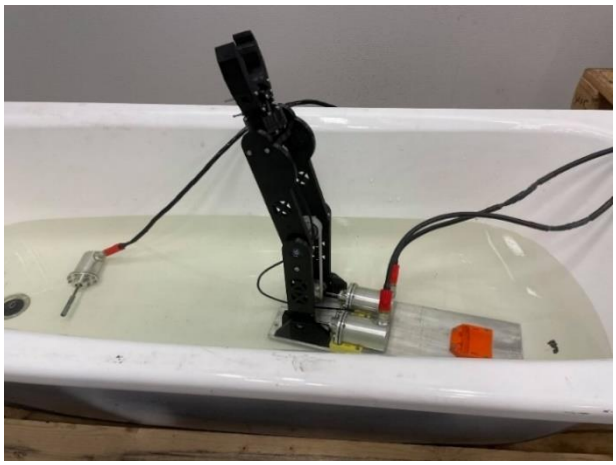

Figure 33 Water test rig

Motors driving link 1 and 2 are installed, while the motor for the grip function is not installed. This motor was not installed due to the steel wire being too short to perform the grip function.

The motors were submerged for approximately 50 minutes while being switched on and off. In the competition the manipulator will be submerged for a maximum of 15 minutes. The test also included lifting a hammer with a weight of 482g, which is approximately 5 N.

3.4 Deflection

The shafts were first 3D-printed in PLA for the first prototype manipulator, but were considered too weak. The deflection when applying a load, was not acceptable and would result in the worm gear pairs to lose contact.

For the final design, the shafts were made in stainless steel with a diameter of 8 mm. The worm gear attached to the lower shaft drives the first link and is labelled number 1. Whereas the worm gear which drives the second link is labelled number 2. The torque provided by gear number 2

is zero as the worm gear is placed on bearings and the torque is instead transferred by a belt to the upper shaft to drive the second link. The lower shaft is therefore not affected by this torque.

The stepper motors maximum output torque will provide the worm gear number 1 with 3,05 Nm on the lower shaft. When using a worm and worm gear to rotate the shaft, the force is acting in the radial, tangential, and axial direction. The decomposed forces and the torque with magnitudes are in Table 4, computed used equations presented in Section 2.4.5. The forces are illustrated in Figure 34. Note that this a worst-case scenario where both worm gears are turning in the same direction.

Table 4 Magnitude of loads on lower shaft

	Worm gear 1	Worm gear 2
Radial force (F_r)	56,6 N	56,6 N
Tangential force (F_t)	152,3 N	152,3 N
Axial force (F_x)	64,1 N	64,1 N
Torque (T)	3,05 Nm	-

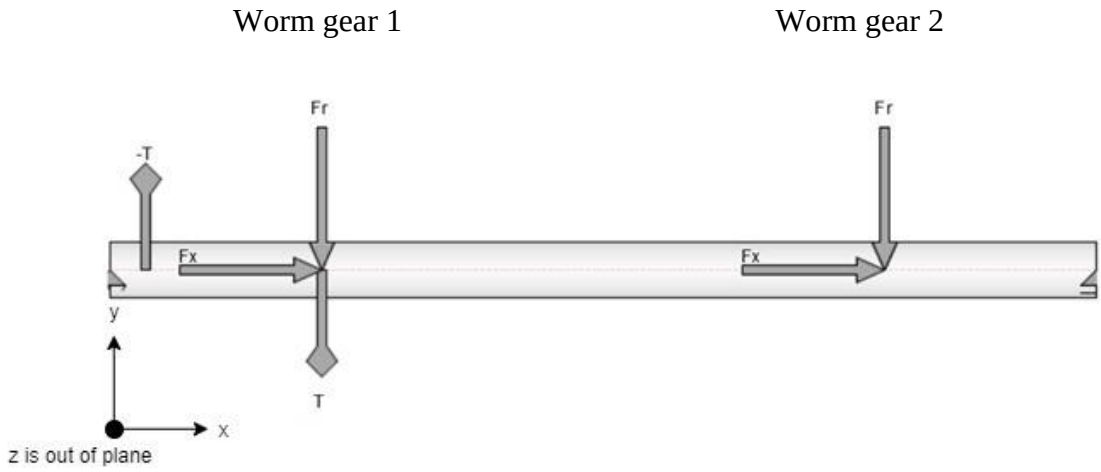

Figure 34 Forces and torque acting on the lower shaft

The tangential forces are placed 90º of the radial force and is placed “behind” the shaft.

3.5 Adams simulation

The exercise was to make the manipulator do a simple task as described below and analyse the kinematics.

The task is illustrated in Figure 35 and is described below

1. Start position should be when both links lie on the x-axis at the coordinate (450, 0)
2. Moving the manipulator over to the object at (200, -200) and pick it up
3. Rotate object 90° using the rotation of the end effector and place the object at (150, 300)

Assumptions

- Land environment
- Only force acting is gravity

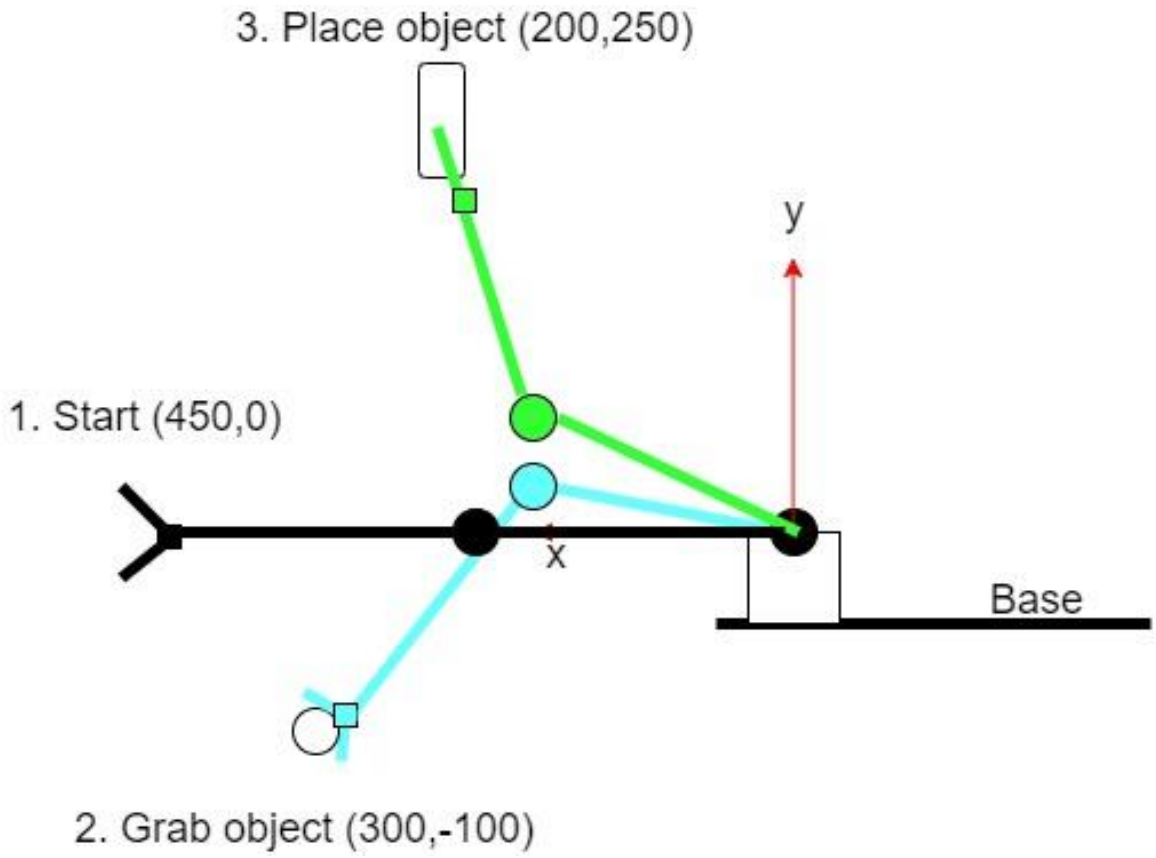

Figure 35 Course of action for the Adams simulation

For the Adams simulation to work, the angles for the different positions are needed. These are computed using Eq. (10) and Eq. (11) and presented in Table 5.

Table 5 Inverse kinematics angles

Angle q_i	Position 1	Position 2	Position 3
q_1	0	25,5°	5,8°
q_2	0	-82,3°	80,6°

The manipulator in the Adams work environment is shown in Figure 36. The model was imported into Adams using Solid Edge. Autodesk Inventor did not export the assembly as separate parts, whereas Solid Edge did this. Having the assembly imported as separate parts made the simulation possible.

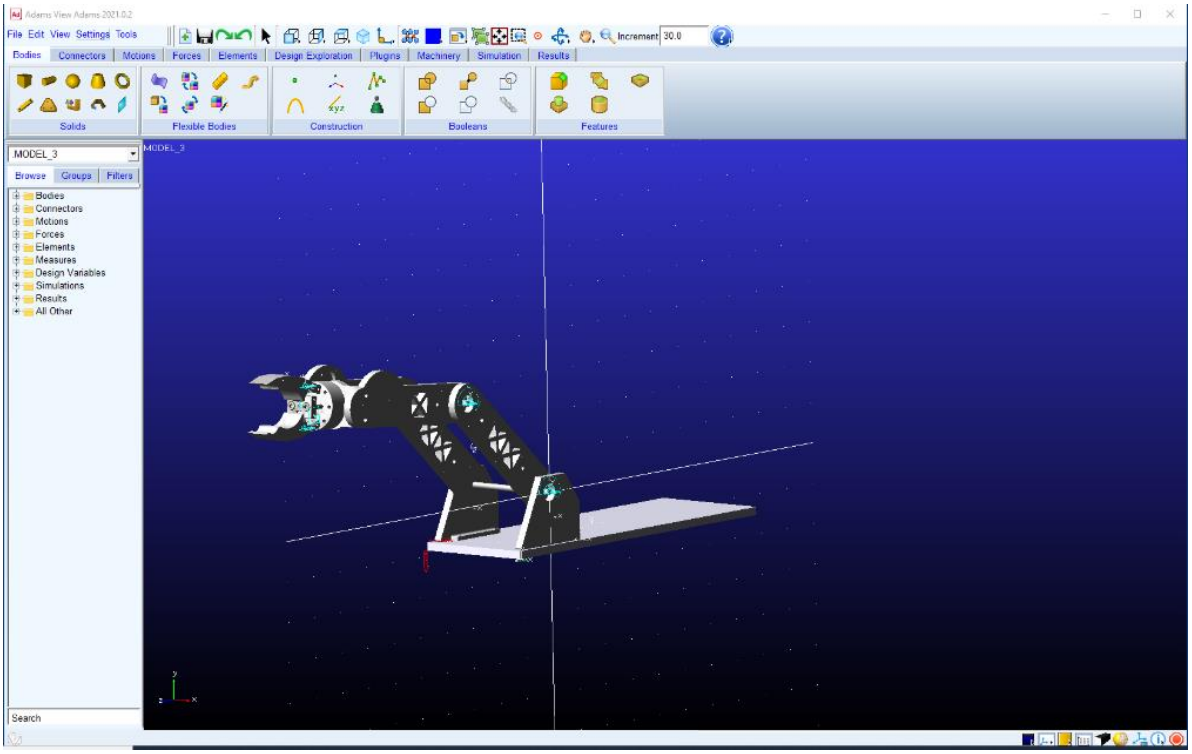

Figure 36 Manipulator in Adams work environment

4. Discussion of Results

This chapter is a presentation of the results for the project, first presenting the manipulator, its workspace, DOFs, functions and components. Adams results will be presented, followed by torque calculations and failures. Figure 37 shows the ROV with the manipulator installed.

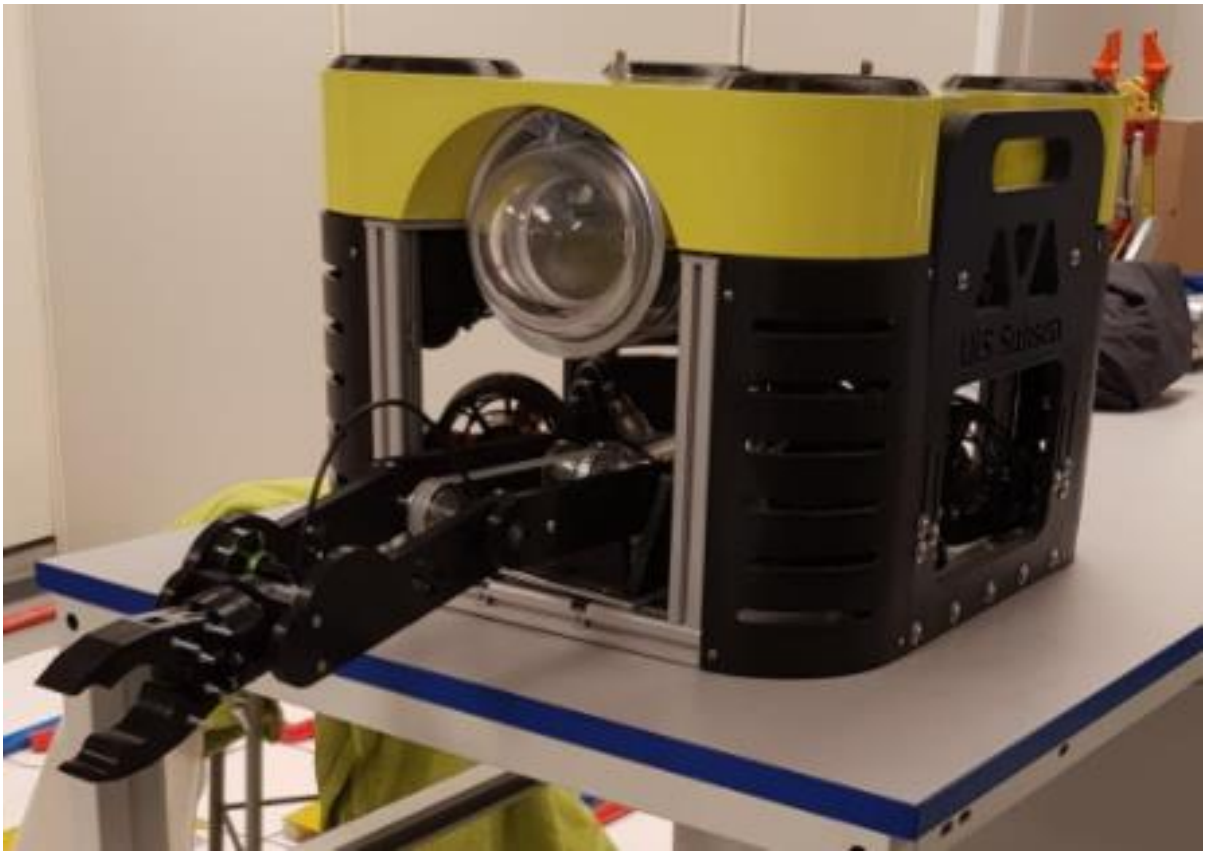

Figure 37 ROV without electrical components

There is no electrical equipment installed at the time this picture was taken, because of delivery problems. A mini ROV will be installed underneath the ROV, in its own docking station. The manipulator will give the ROV a good overall reach, while providing the necessary functions for completing the tasks at hand.

4.1 Final design

The final design of the manipulator has three DOF; two main joints and a rotational end effector. This design can execute all the relevant tasks defined in the MATE manual.

The movements in the two main joints are made by two worm gear pairs. Worm gear pairs do not rely on the motors to hold the moment of the manipulator, it is held by the friction between the pair. The manipulator is therefore able to be positioned in any position without any load on the motors. Figure 38 displays the manipulator with numbered components, the numbers are explained below

To make the movement on the lower arm, the worm gear ① is attached into the lower shaft with set screws and press fit. The set screws were placed as a safety in case the press fit slips due to reduced friction in water.

To move the upper arm, a belt and belt pulley were used. The belt pulley is directly attached to the worm gear ② and will rotate when the worm gear rotates. However, the worm gear and belt pulley can rotate independently of the lower shaft due to them being placed on bearings as shown in Figure 39 on the next page.

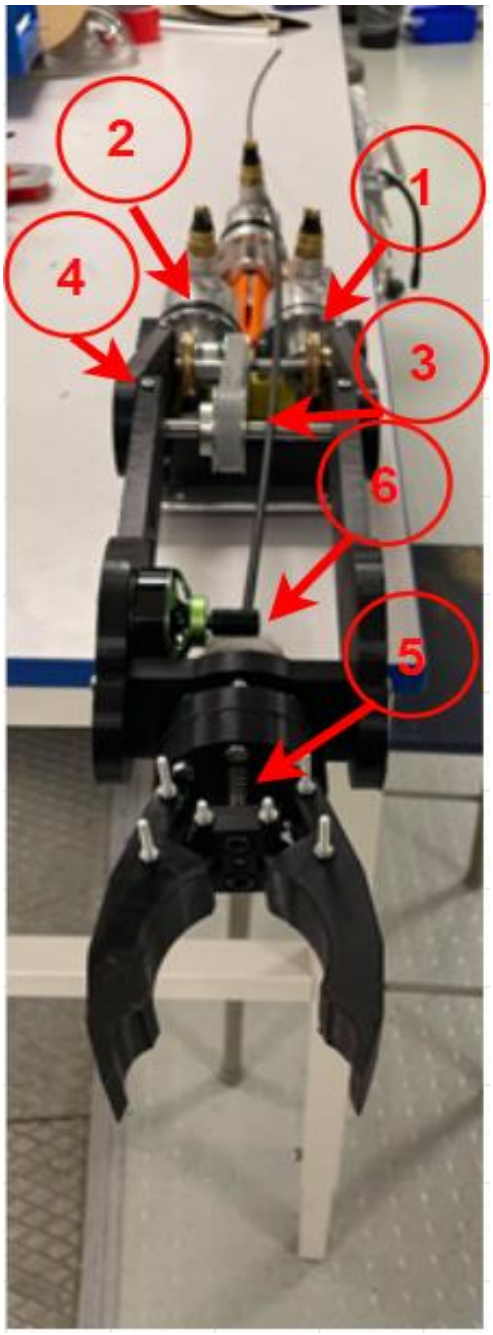

Figure 38 Manipulator front view

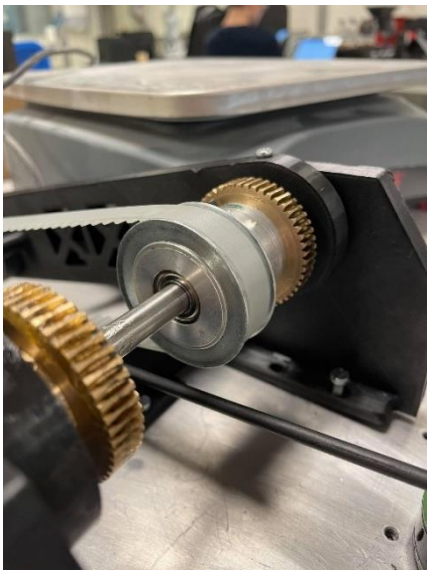

Figure 39 Gear / pulley / bearing setup

The belt pulley on the upper shaft ③ is attached with a press fit and will rotate the second joint when the belt is moved. Because PLA and metal do not make a firm press fit, screws were placed in the side plates of the lower and upper arm into the shafts which were threaded ④.

A wire runs through the manipulator and is placed in the centre of the rotational end effector joint so it can rotate without any limits when the wire is being pulled. The wire makes the end effector grip. Using two springs used as counter force to pull the wire in the opposite direction for the end effector to open when the wire tension is released ⑤.

The rotational end effector joint has a worm gear attached at the end ⑥. A motor mounted perpendicular to the rotational joint is fitted with a worm on the shaft and will make the end effector rotate when the motor starts.

Bearings are placed in both the joints of the lower and upper arm and on the rotational end effector joint. The front bracket has two small bearings where the shafts from the motors are placed.

All nonstandard parts are 3D-printed in PLA to make the manipulator as light as possible to keep the ROV within the limit of 35 kg. The bottom plate is in aluminium, and the worm gears are in bronze, both which can handle humid environments well.

Figure 40 displays the manipulator from another angle. Note that the wire was not installed and the bolts on the gripper was not of the correct dimension at the time of this picture.

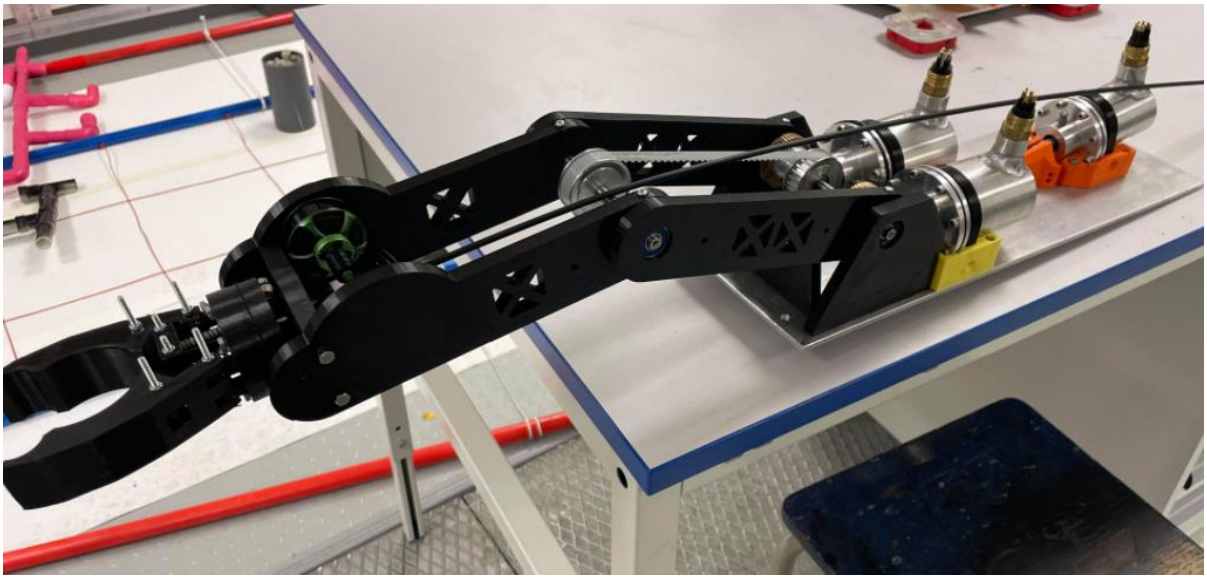

Figure 40 Manipulator side view

Figure 41 displays the base plate without the manipulator installed. Note that the wing nuts placed in each corner provide an easy modular design and the motors are placed behind the manipulator, acting as counterweights.

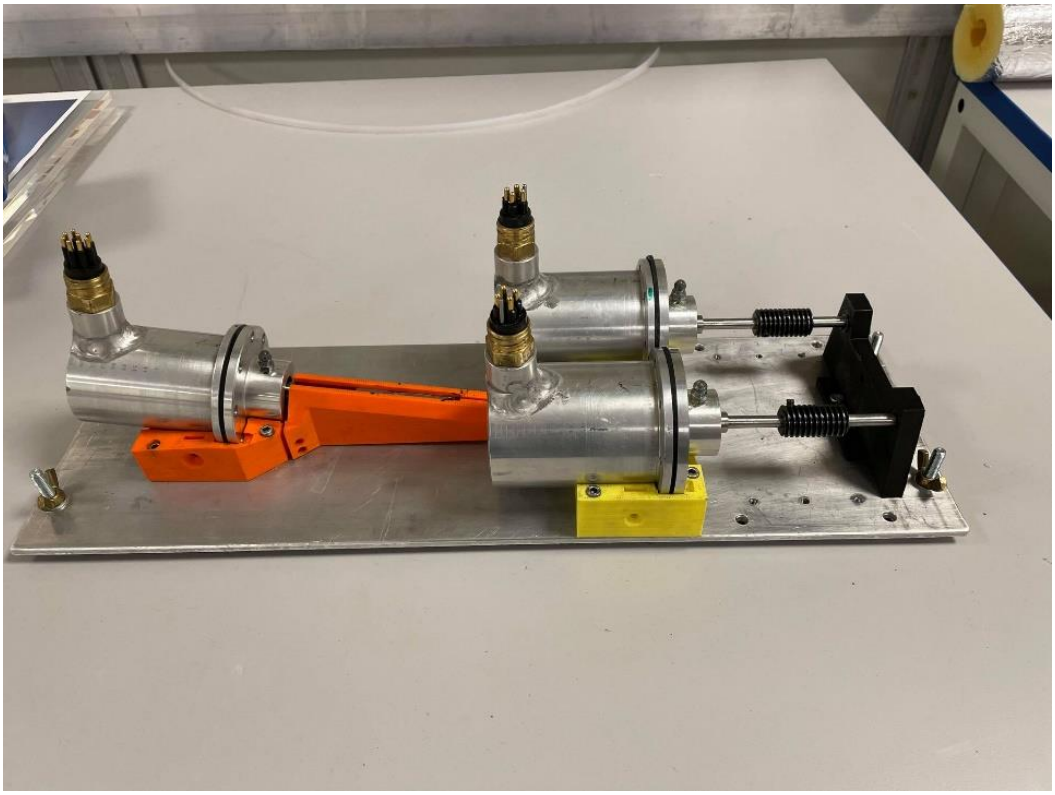

Figure 41 Base plate

The final design combined with the motors and worm gears, makes it possible to create a theoretical load capacity diagram, dependent on the position of the manipulator. This load illustration in Figure 42 is based on dry conditions on land, where the friction coefficient between steel and bronze on the worm and worm gear is at its highest, $\mu = 0.34$ [28].

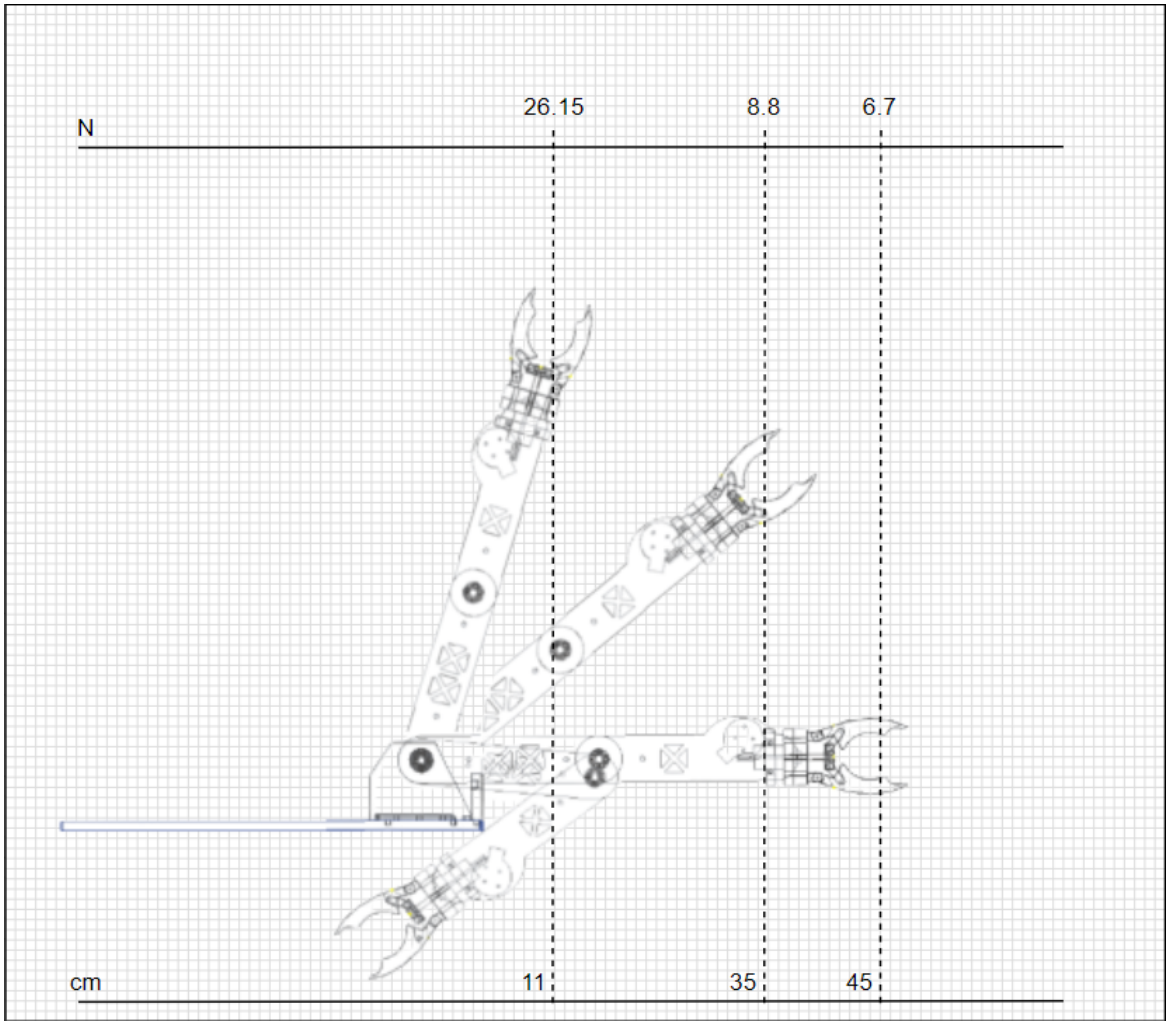

Figure 42 Load illustration of the manipulator

The figure shows what the lifting capacity is at 45 cm, 35 cm, and 11 cm reach. Which correspond to angles of respectively 0, 40 and 75 degrees. This results in a lifting capacity of 6.7 N, 8.8 N and 26.15 N. The lifting capacity increases when the angle increases.

The friction coefficient could be reduced in water during wet conditions, but no exact value was found. If the friction coefficient should be reduced, the motor load would be reduced, and the manipulator would have an increased lifting capacity.

The gripper is shown in an open and closed position in Figure 43 (a) and (b) respectively.

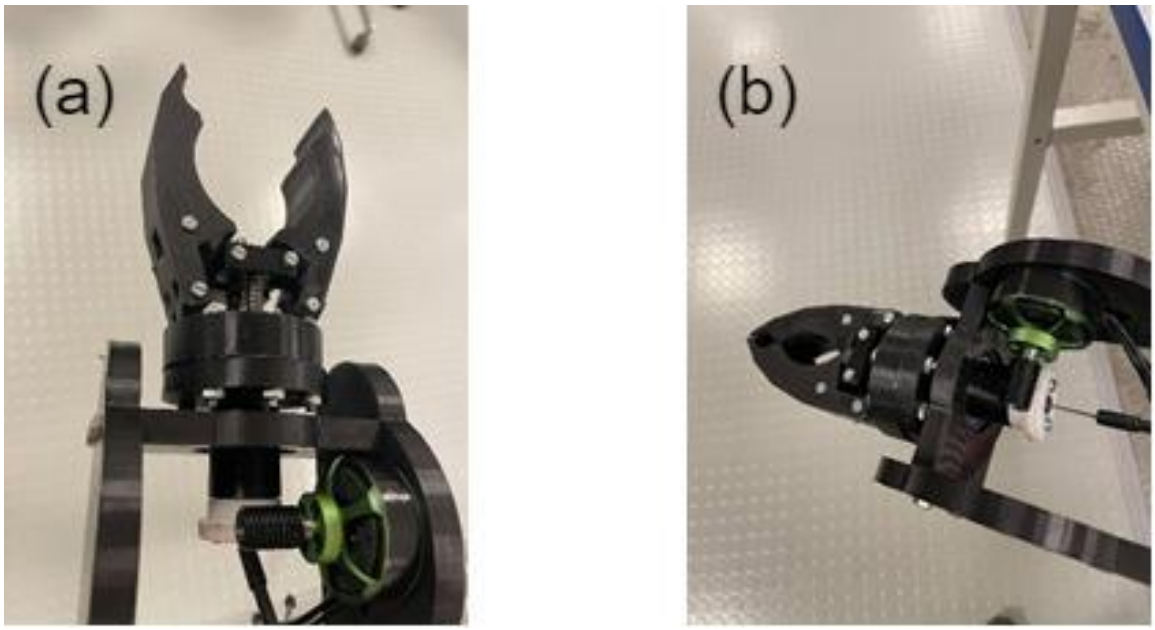

Figure 43 Open and closed gripper

The gripper can grasp and hold a 60 mm motor which is roughly equal to the OD of the largest pipe at 60,3 mm. The smallest pipe for the gripper to hold has an OD of 21 mm, and the gripper can hold a 17 mm marker. This proves that the gripper will be able to hold both the largest and smallest pipes in the competition, shown in Figure 44.

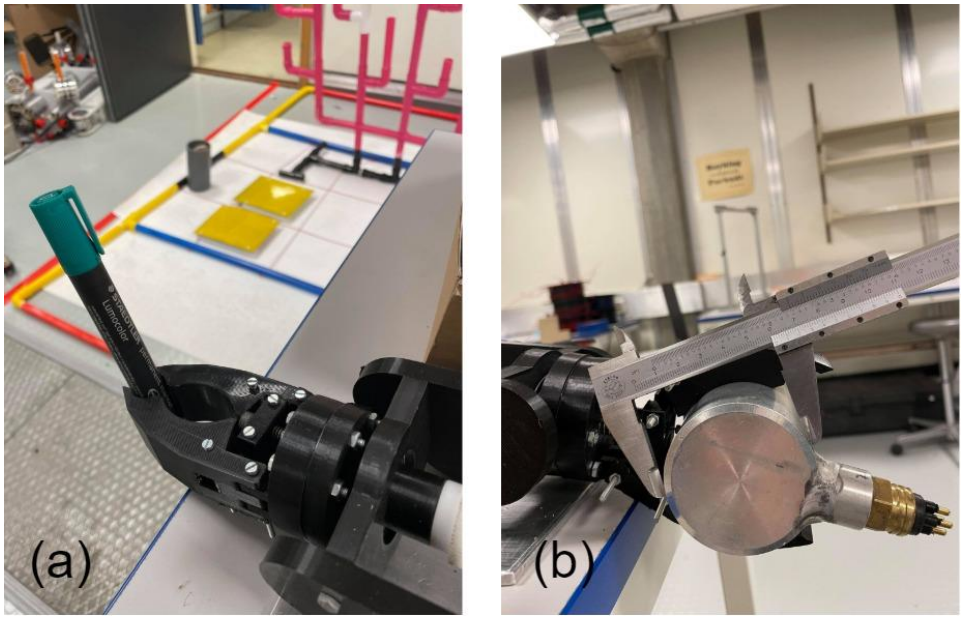

Figure 44 (a) 17 mm marker, (b) 60 mm motor housing

The gripper is able to fully close, leaving no room for the rope, zip-lock bag or the 5 mm pin to slip, as shown in Figure 45.

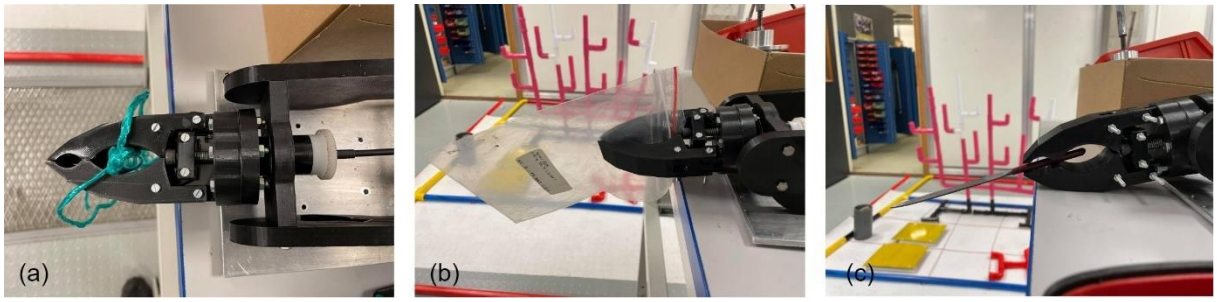

Figure 45 (a) Rope, (b) Zip-lock, (c) 5 mm pin

Figure 46 shows the total workspace of the manipulator and three positions. A workspace of a planar robot arm was generated using a MATLAB code from Al-Fetyani [29].

The following constraints were in place

- No end effector attached
- Link length 225 mm
- $-10° \leq q_1 \leq 90°$
- $-120° \leq q_2 \leq 90°$

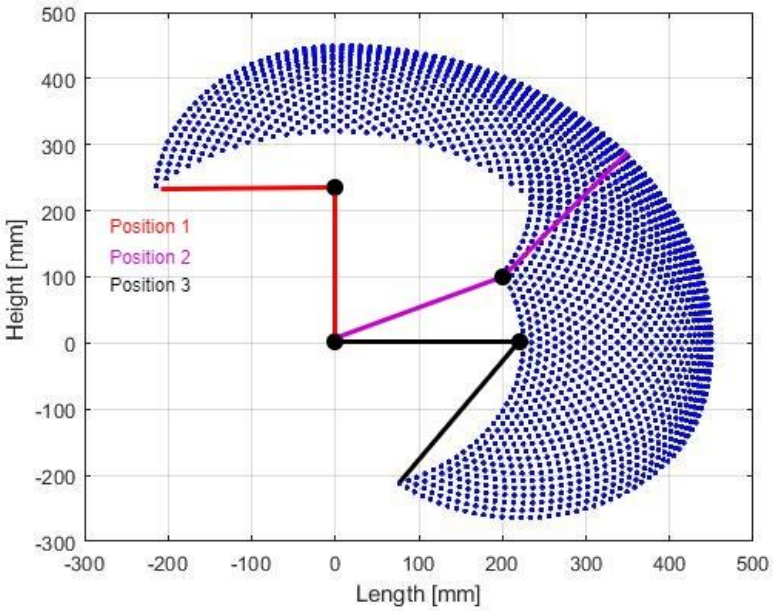

Figure 46 Workspace of a planar robot arm

The workspace is clearly enough, and when installed on the ROV, the manipulator will be able to move around and operate in a 3D environment.

Figure 47 displays the manipulator without motors or gears installed. The icons ranging from 1-13 are explained in Table 6.

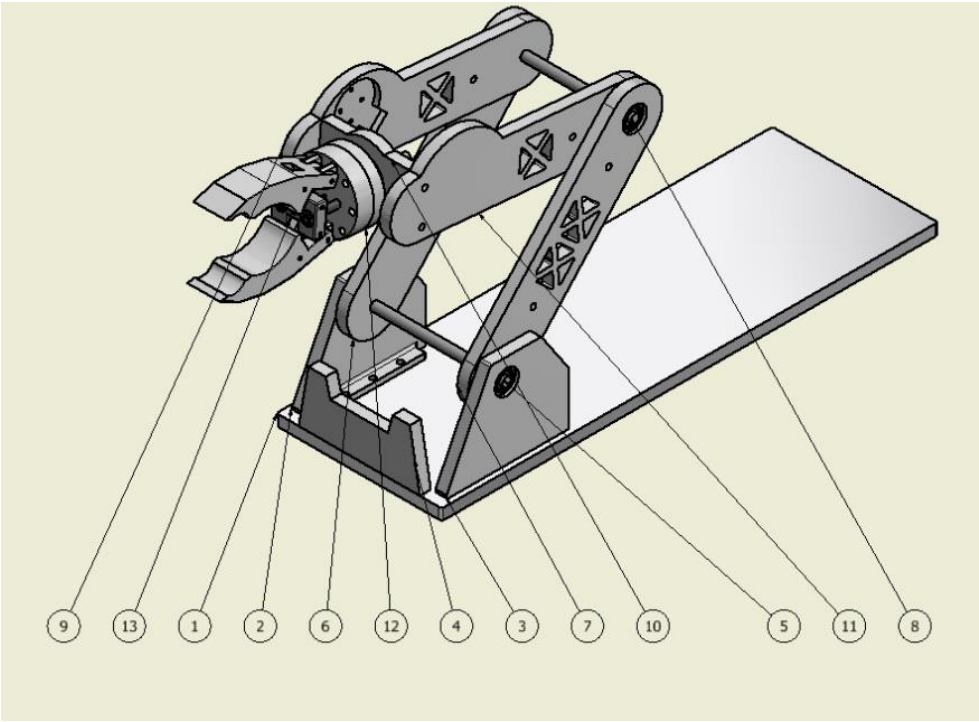

Figure 47 Manipulator without motors or gears

Table 6 Manipulator icon names

Build:	**Part number:**	**Name:**
Base	1	Bottom plate
	2	Right side bracket
	3	Left side bracket
	4	Front bracket
Lower arm	5	Lower shaft
	6	Right side plate
	7	Left side plate
Upper arm	8	Upper shaft
	9	Right upper plate
	10	Upper bracket
	11	Left upper plate
	12	Rotational joint
Gripper	13	Gripper

4.2 Weight and size

The ROV must not exceed the weight limit of 35 kg and must have a diameter smaller than 92 cm. The project focused on these two requirements as they would lead to disqualification.

When measuring the diameter of the ROV, modular parts can be placed on top of the ROV. Therefore, it was decided to make the manipulator modular which would reduce the overall ROV diameter when not installed as shown in Figure 48.

Figure 48 Manipulator on top of ROV

The company decided to use thrusters designed for kayaks at a weight of 0,6 kg each, and because there are 8 of these, it sums up to 4,8 kg. The electronic housing is made of aluminium instead of plastic, requiring more of the weight budget than previous years. It was therefore crucial to reduce the weight of the manipulator as much as possible. This led to the goal of reducing the weight by 40% compared to the 2015 version. This was achieved by removing the three largest motors, Nema 24, and by replacing most aluminium parts with 3D printed PLA parts.

This year's manipulator weighed 4,855 kg, while that of 2015 weighed 8,802 kg as shown in Figure 49 and Figure 50 respectively.

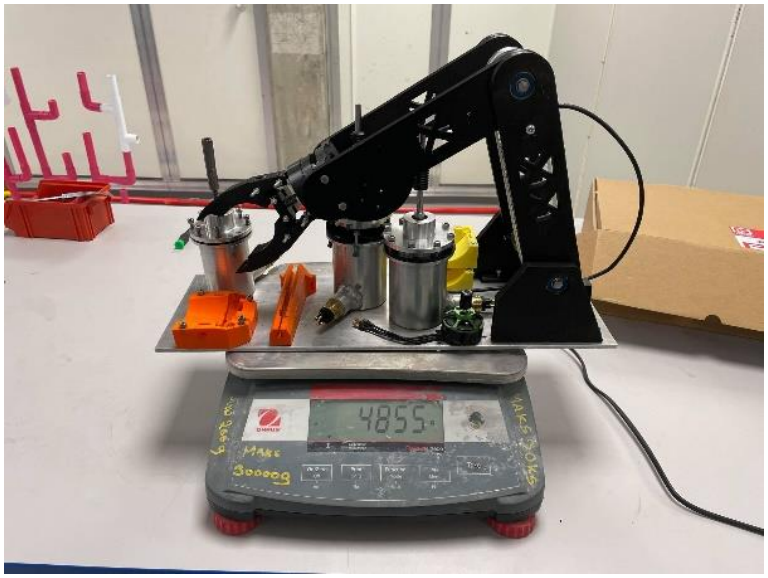

Figure 49 2021 Manipulator weight

Figure 50 2015 Manipulator weight

Then the weight reduction in percentage is

$$\%\, reduction = \frac{8802 - 4855}{8802} * 100\% \approx 45\% \tag{45}$$

45% weight reduction is a satisfying result while only sacrificing one DOF, because the end effector cannot tilt.

The space where the manipulator is going to be installed, is limited to a width of 150 mm. This year's manipulator has a width of 150 mm, while the 2015 manipulator has a width of 330 mm. Shown in Figure 51 and Figure 52 respectively.

Figure 51 2021 Manipulator width

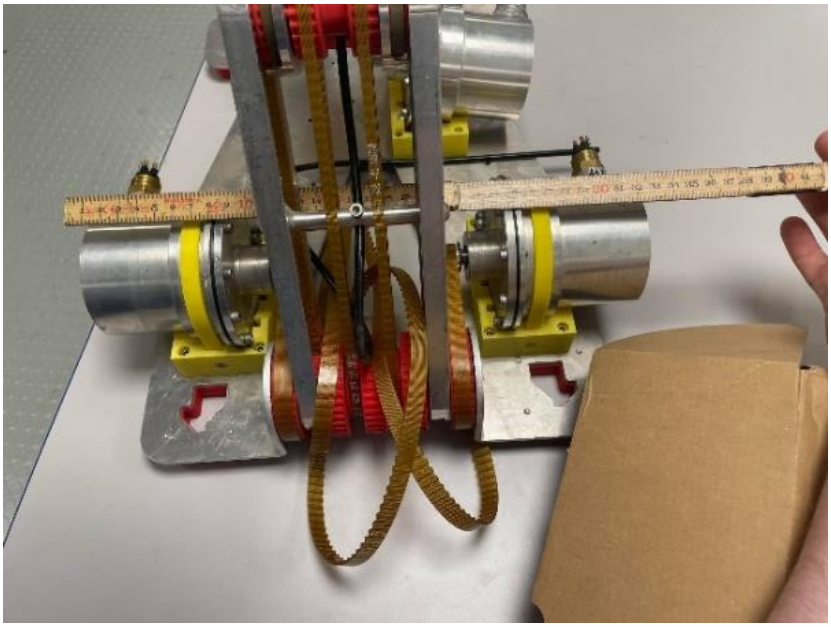

Figure 52 2015 Manipulator width

The width of the 2015 version is caused by the placement of the motors. Instead of having the motors installed facing each other, they were installed parallel on the 2021 version. This meant the width could be reduced to 150 mm. In total a reduction in width of 190 mm.

The overall reach of the arm has not changed much. The centre of the gripper is almost the same at approximately 450 mm. Figure 53 and Figure 54 shows the new reach and old reach respectively.

Figure 53 2021 Manipulator reach

Figure 54 2015 Manipulator reach

4.3 Motor specifications

The choice of motors are as follows

- Nema 17, 17HS24-2104S to drive link 1
- Nema 17, 17HS24-2104S to drive link 2
- Nema 14, 14HS20-1504S to drive grip function
- Multistar Elite 3508-268KV to drive the rotation of the end effector, link 3

The motors will run at 12 V, simplifying the setup for the electrical team.

Calculations for the worm gear pairs is based on the theory presented in Section 2.4.5 and calculations of angular velocities is based on Section 2.4.8.

BLDC motor

The Multistar Elite 3508-268KV has a KV rating of 268 which gives the theoretical max RPM

$$RPM_{max} = 268\ KV * 12\ V = 3216\ RPM \tag{46}$$

and theoretical max angular velocity

$$\omega_{3,max} = 3216\ RPM * \frac{\pi}{30} = 337 \frac{rad}{s} \tag{47}$$

The motor is connected to a worm gear pair that has a gear ratio of 1:60 and this will give a maximum angular velocity for the end effector of

$$\omega_{3,out} = \omega_{3,max} * \frac{1}{60} = 5{,}6\ \frac{rad}{s} \tag{48}$$

The control system allows the BLDC motor to achieve all values up to and including the above angular velocity.

The BLDC has a maximum current of 12 A whilst running at 12 V. This results in the effect

$$Q = 12\,V * 12\,A = 144\,W \tag{49}$$

and therefore, the maximum torque of the motor is

$$T_{max} = \frac{Q}{\omega_{3,max}} = \frac{144\,W}{337\,\frac{rad}{s}} = 0{,}43\,Nm \tag{50}$$

The worm attached to the BLDC motor is a SUW0.5-R1 and is connected to a DG0.5-60R1 worm gear. Values for the worm and worm gear is shown in Table 7.

Table 7 Steel-Nylon worm gear pair dimensions

Type	Unit	Worm SUW0.5-R1	Worm gear DG0.5-60R1
Material	-	Steel	Nylon
Number of teeth	-	1	60
Module	$[mm]$	0,5	0,5
Diameter	$[mm]$	12	31
Reference angle	$[deg]$	20	20

The lead angle for the steel worm SUW0.5-R1 paired with the nylon worm gear DG0.5-60R1 is computed using Eq. (20)

$$\gamma = \tan^{-1}\left(\frac{0{,}5 * 1}{12}\right) = 2{,}4° \tag{51}$$

Inserting values into Eq. (19) yields

$$0{,}4 \geq 0{,}04 \tag{52}$$

and therefore, this worm gear pair is self-locking, allowing the BLDC motor to exploit this property.

Friction between nylon and steel is assumed to be $\mu = 0{,}4$ [30]. Inserting values into Eq. (22), Eq. (23) and Eq. (24), yields an output torque of $T_{out} = 2{,}3\,Nm$.

Nema 17 stepper motors

The Nema 17 succeeded in lifting the 1774 g nut, as shown in Figure 55 .

Figure 55 Nema 17 lifting 1774 g at 250 mm

This results in a lift capacity of

$$Lift\ capacity = 9{,}81\frac{m}{s^2} * 1{,}772\ kg = 17{,}38\ N \tag{53}$$

This implies that the Nema 17 can lift an object that is at least 70% heavier than necessary. Therefore, the stepper motor Nema 17 is suited for lifting 5 N at 500 mm reach.

The test described in Section 3.2 implied that the highest torque was achieved at the resolution

$$S = 12800\ \frac{steps}{rev} \tag{54}$$

For both Nema 17 stepper motors, the electrical team found that these should have a frequency that lies within the range of [20]

$$153\ Hz < frequency < 65359\ Hz \tag{55}$$

The angular velocity in both links can vary between the minimum and maximum angular velocity. The belt transmission runs on two identical pulleys, and Eq. (13) yields that $i_{transmit} = 1$, therefore both link 1 and 2 will have the same minimum and maximum angular velocities. With a gear ratio of 1:50, the minimum angular velocity is

$$\omega_{1,2\,min} = \frac{2\pi * 153\ \frac{steps}{s}}{12800\ \frac{steps}{rev}} * \frac{1}{50} = 0{,}0015\ \frac{rad}{s} \tag{56}$$

and the maximum angular velocity is

$$\omega_{1,2\,max} = \frac{2\pi * 65359\ \frac{steps}{s}}{12800\ \frac{steps}{rev}} * \frac{1}{50} = 0{,}64\ \frac{rad}{s} \tag{57}$$

Calculating the maximum torque of a stepper motor is not possible and instead the datasheet for the specific motor should be used. See Figure 56 for the torque curve of the Nema 17HS24-2104S.

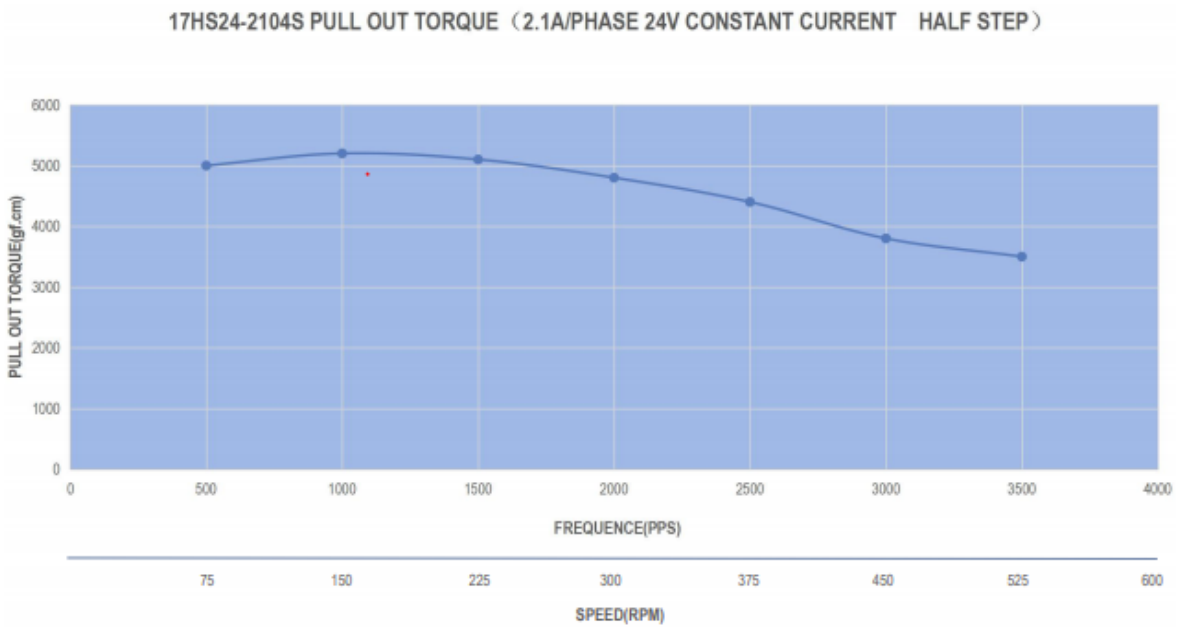

Figure 56 Torque curve 17HS24-2104S [31]

By inspection, the maximum available torque is approximately 0,5 Nm

The worm attached to the Nema 17 stepper motor is a SWB08/R1 and is connected to a BWW08/50/1R worm gear. Values for the worm and worm gear is shown in Table 8.

Table 8 Steel-Bronze worm gear pair dimensions

Type	Unit	Worm SWB08/R1	Worm gear BWW08/50/1R
Material	-	Steel	Bronze
Number of teeth	-	1	50
Module	$[mm]$	0,8	0,8
Diameter	$[mm]$	15,6	41,6
Reference angle	$[deg]$	20	20

The lead angle for the steel worm SWB08/R1 paired with the bronze worm gear BWW08/50/1R is computed using Eq. (20)

$$\gamma = \tan^{-1}\left(\frac{0{,}8 * 1}{15{,}6}\right) = 2{,}9° \tag{58}$$

Inserting values into Eq. (19) gives

$$0{,}34 \geq 0{,}05 \tag{59}$$

therefore, this pair is self-locking, allowing the Nema 17 stepper motors to exploit this property.

Friction between bronze and steel is assumed to be $\mu = 0{,}34$ [28]. Inserting values in Eq. (22), Eq. (23) and Eq. (24) yields an output torque for the worm gear of $T_{out} = 3{,}0\ Nm$. Further proving that the Nema 17 can lift 5 N at 0,5 m. Because

$$F_{max,lift} = \frac{T_{out}}{max\ reach} = \frac{3{,}0\ Nm}{0{,}5\ m} = 6\ N \tag{60}$$

If the lift capacity found in the test is converted into torque

$$T_{lift} = lift\ capacity * test\ reach = 17{,}38\ \text{N} * 0{,}25\ \text{m} = 4{,}35\ Nm \tag{61}$$

Comparing this against the torque found by using the datasheet

$$T_{lift} > T_{out} \tag{62}$$

This implies that the motor has an output torque higher than specified in the datasheet. The most probable reason for this is in gear transmission, where the output torque in the datasheet assumes a worst case scenario friction coefficient. It is possible to compute the real friction coefficient.

If all other parameters are assumed to be constant, that is

- $\gamma = 2{,}94°$
- $\alpha = 20°$
- $T_{lift} = 4{,}35\ N\ m$, from the lift test
- $T_{max} = 0{,}5\ Nm$, from the datasheet

By solving for μ in Eq. (22) , the real friction coefficient may be written as

$$\mu_{real} = \frac{F_{t1}\cos\alpha\cos\gamma - F_{t2}\cos\alpha\sin\gamma}{F_{t2}\cos\gamma + F_{t1}\sin\gamma} \tag{63}$$

where the tangential component on the worm is found by using Eq. (23)

$$F_{t1} = \frac{T_{max} * 2}{d_1} = \frac{0{,}5\ Nm * 2}{0{,}0156\ m} = 64{,}1\ N \tag{64}$$

and the tangential component on the worm gear is found by solving for F_{t2} in Eq. (24)

$$F_{t2} = \frac{T_{lift} * 2}{d_2} = \frac{4{,}35\ Nm * 2}{0{,}04\ m} = 217{,}5\ N \tag{65}$$

The real friction coefficient by Eq. (63) is then

$$\mu_{real} = 0{,}2254 \tag{66}$$

It can be seen that μ_{real} is lower than the assumed coefficient of friction. However, the friction may not be the whole reason for the increased lift capacity. There may be installation errors or other unknown factors.

Nema 14 stepper motor

For the Nema 14 stepper motor that creates the grip force, it makes no sense to speak in terms of angular velocity and the only parameter which is necessary is the max pull force, which is equal to 170 N [10, p. 28].

Figure 57 shows the different measurements needed to calculate the spring force and the grip force.

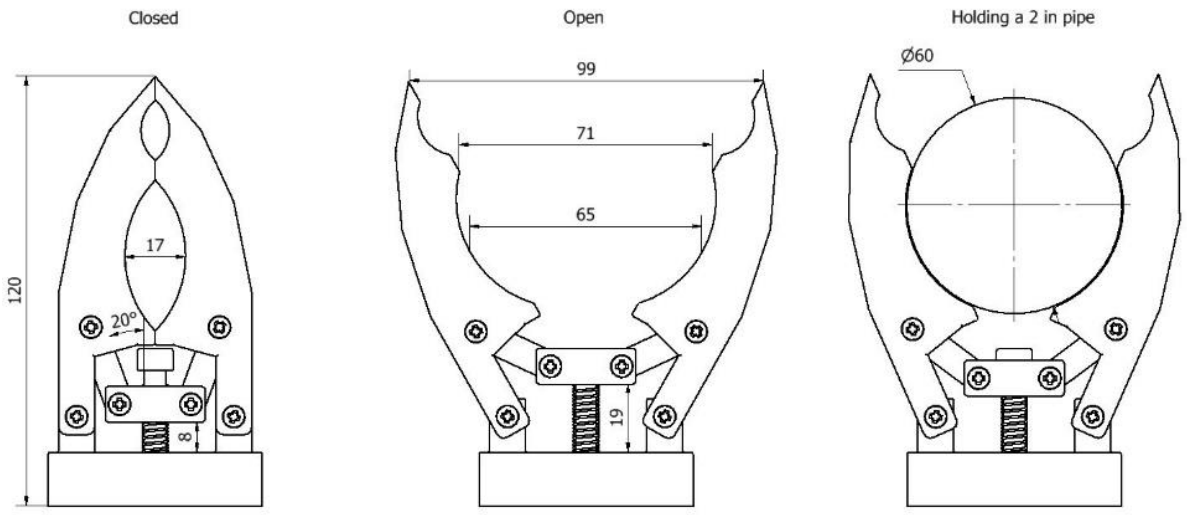

Figure 57 Measurements of the gripper

The springs used are stainless compression springs with a spring constant of $k = 0{,}11\frac{N}{mm}$. It was only possible to buy springs having a length of 65 mm. The springs was therefore cut down to 25 mm to ensure there is always some force acting.

Using the theory presented in Section 2.4.2. The force of the springs when the gripper is in an open position is

$$F_{open} = (25 - 19)\ mm * 2 * 0{,}11 \frac{N}{mm} = 1{,}32\ N \tag{67}$$

and for the closed position the force of the springs is

$$F_{closed} = (25 - 8)\ mm * 2 * 0{,}11 \frac{N}{mm} = 3{,}74\ N \tag{68}$$

As there is close to no friction inside the wire protection, these forces should be enough to open the fingers when the motor is releasing the tension. Using the theory presented in Section 2.3, the max grip force when taking the springs into account for a closed position is

$$F_{grip,max} = \frac{(170\ - 3{,}74)\ N}{2} * \tan(20°) = 30\ \text{N} \tag{69}$$

By comparison the heaviest load is 5 N. Therefore, the motor should be able to hold the object without the fingers opening. The gripper can rotate which allows it to position itself such that the object in hand cannot slip out of the grip. The minimum force that the Nema 14 motor must apply to hold 5 N is

$$F_{applied,min} = 2\left(\frac{5}{\tan(20°)} + \frac{3{,}74}{2}\right) N = 32\ \text{N} \tag{70}$$

It is possible to calculate the torque required by the motor to exert 32 N in the wire. By modelling the connection as a wire attached to a nut which can travel up and down a screw. As illustrated by Figure 58.

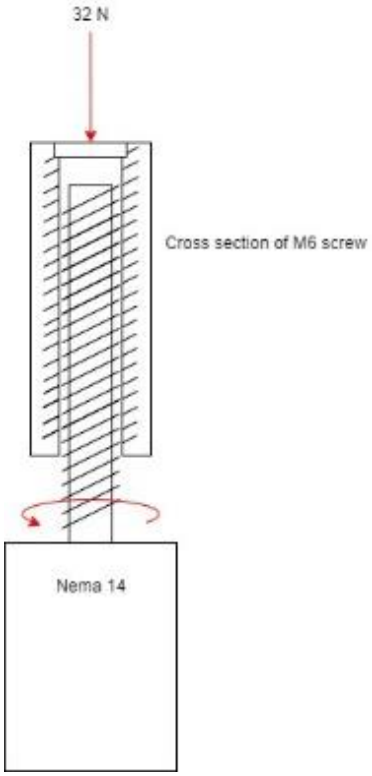

Figure 58 Model of a screw pulling a weight

The torque required to achieve this force may be written as [17, p. 98]

$$T_{grip,min} = F_{applied,min} * r * \left(\frac{\mu_s + tan\gamma}{1 - \mu_s tan\gamma}\right) \tag{71}$$

The screw is a M6 with dimensions

Radius, $r = 3\ mm$

Lead angle, $\gamma = 3{,}04°$

Friction coefficient steel on steel, $\mu_s = 0{,}42$ [30]

Inserting values into Eq. (71) gives $T_{grip,min} = 46\ Nmm$. Comparing this to the torque curve of the Nema 14 motor shown in Figure 59, it will be able to apply this torque at all levels available.

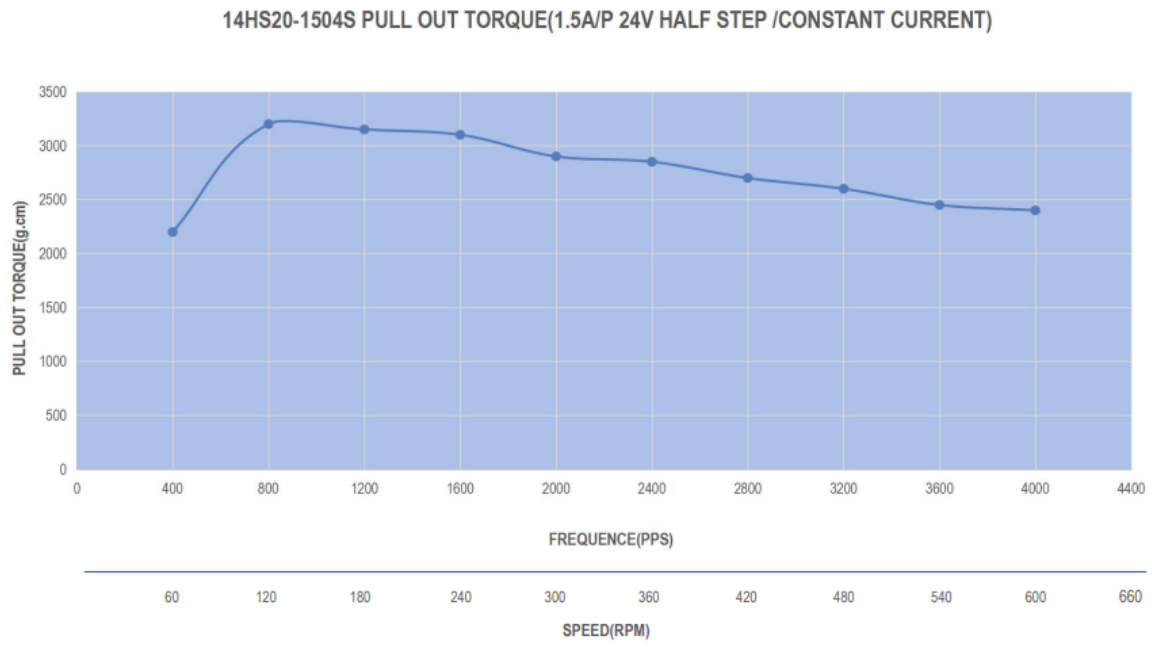

Figure 59 Torque curve 14HS20-1504S [32]

4.4 Waterproof

The manipulator successfully lifted the 482 g hammer and there were no signs of leakages from the test in Section 3.3. Figure 60 displays each stepper motor after the bathtub test and clearly show no signs of leakage.

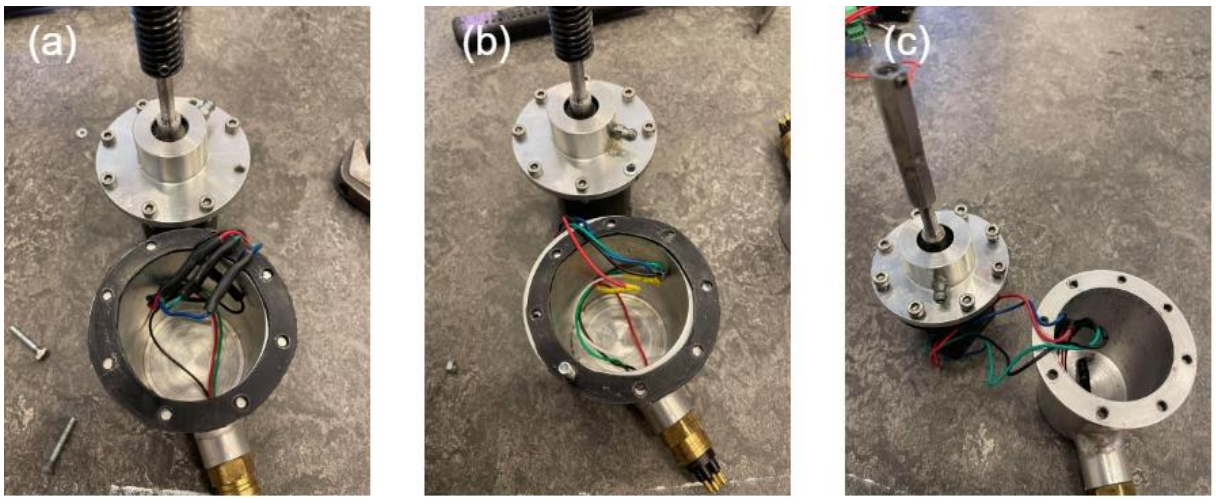

Figure 60 (a) Nema 17, (b) Nema 17, (c) Nema 14

The test included the BLDC motor Multistar Elite 3508-268KV. The coils are coated with epoxy and should be waterproof because they are not in contact with the water. The motor was

not installed on the manipulator during the test due to the electrical wires being too short, as shown in Figure 61. The test was sufficient and proved that the epoxy coating was ok.

Figure 61 Waterproof BLDC motor

The project did not have access to connectors that could reach the required depth of 5-10 m and the ROV was not finished at the time of testing. This led to the waterproof test only being done in a bathtub. However, this test is not sufficient to conclude that the seals are waterproof at the required depth. As the motors are only slightly submerged it is possible to approximate the pressure as being the same as the atmospheric pressure at sea level.

$$P_{atm} = 1\ bar \tag{72}$$

If the manipulator was submerged to the maximum required depth of 10 m, the pressure would be approximately doubled.

$$P_{10\ m} = P_{atm} + \rho_{H2O} * g * depth\ \approx 2\ bar \tag{73}$$

This would increase the pressure on the seals as well by a factor of two. It is therefore necessary to test at a pressure of 2 bar. The project was not able to do this before 15th of May due to the other parts of the ROV not being complete. It would have been possible to test in a pressure chamber, but this would require much resources at this time. It is therefore more reasonable to wait for the ROV to be complete before further testing of the seals.

Table 9 is the documentation from the 2015 manipulator [10, p. 11]. This year's manipulator is using the same methods and housings and it is therefore reasonable to assume the data below still holds.

Table 9 2015 Waterproof documentation

Test number	Depth	Time	Rotation	Comment
1	20 m simulated	25 min	Continuous	No sign of failure
2	50 m simulated	5 min	Alternating with short stops	Made to fail
3	0,2 m	27 hours	Continuous with long stops	No sign of failure
4	3 m	50 hours	Alternating continuous	No sign of failure
5	0-4 m	6 hours	Normal use of ROV with manipulator	No sign of failure

4.5 Deflection results

The deflection in the lower shaft caused by all these forces can be measured in micrometres, and the highest value is 272 micrometres, and is shown in Figure 62. The deflection in the YZ-plane and XZ-plane can be seen in Figure 63 and Figure 64 respectively.

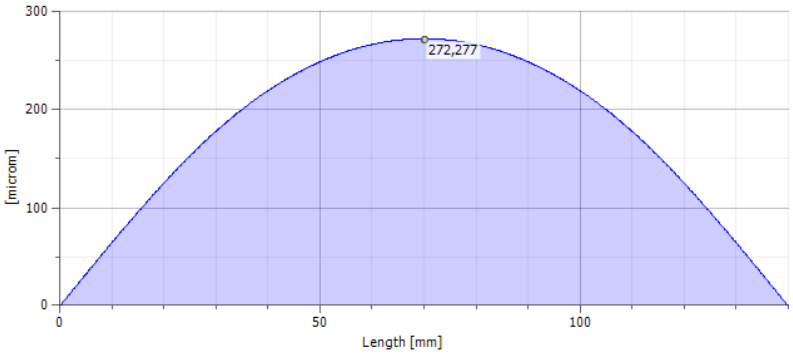

Figure 62 Magnitude of deflection

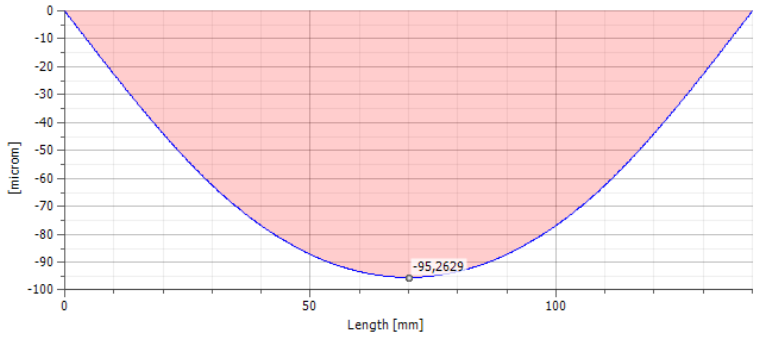

Figure 63 YZ deflection

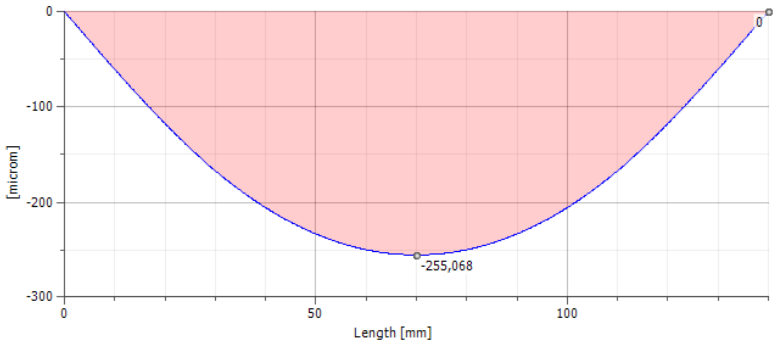

Figure 64 XZ deflection

Most forces are acting upon the lower shaft, and because the displacement is not severe, the upper shaft is able to handle the load because there are less forces acting upon it.

4.6 Adams simulation results

The following Figure 65, Figure 66 and Figure 67 displays the results from Adams in terms of position, velocity and acceleration respectively. Notes for reading the position graph

- Y-axis must be corrected by adding 7,5 mm
- X-axis must be corrected by adding 5 mm

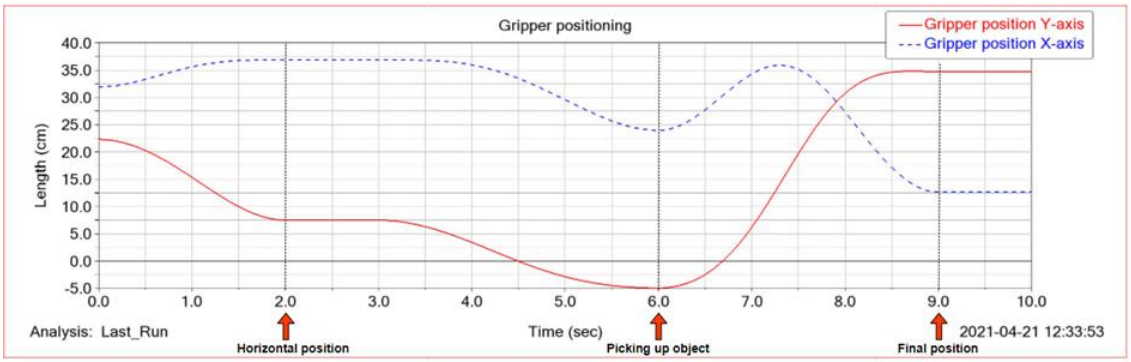

Figure 65 Gripper position

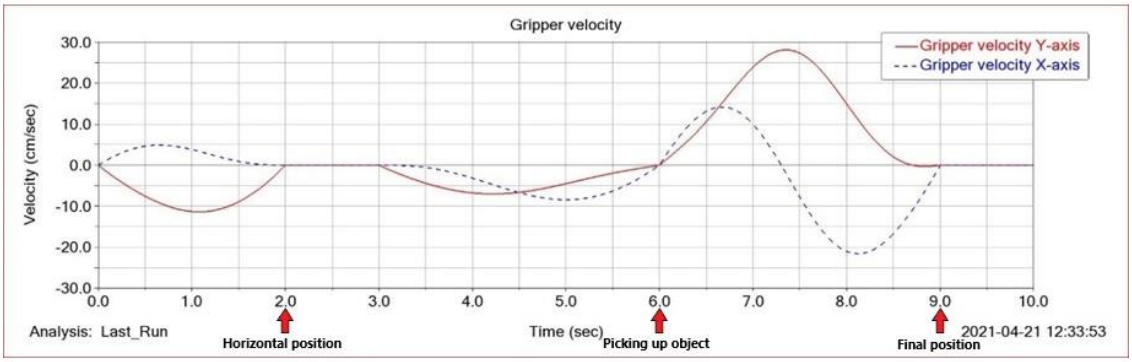

Figure 66 Gripper velocity

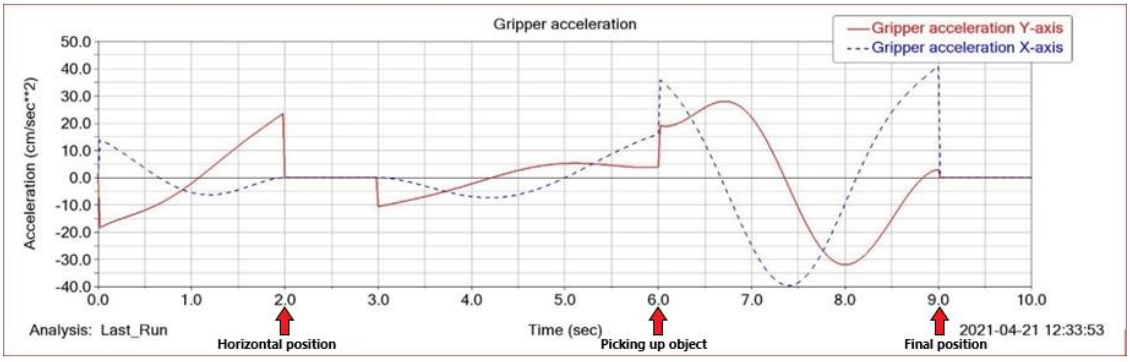

Figure 67 Gripper acceleration

The use of Adams in this thesis is limited to simulating the movement of the arm. Comparing the results regarding position, velocity, and acceleration to calculated theoretically position shows the manipulator is working as intended. The results were as expected, the manipulator works fine in the Adams environment.

The knowledge and experience in using Adams was at a beginner's level, and was learned solely for this thesis, which is reflected in the results. It would have been a more useful tool if the software was implemented at an earlier stage of the education and by having a chance to become more familiar using it.

It is possible to create a flex body system in Adams. This allows the user to simulate loads of each part individually, with a colour coding from green to red, indicating if the structure will be able to withstand the forces acting upon it. This feature was however not used, due to lack of knowledge.

Time was such an important factor for this thesis, with both production and writing there was not enough time available to learn the software beyond beginner's level. Adams has proven to be a powerful tool in the process of designing and simulating new components and parts interacting with each other. Unfortunately Adams was not used to its fully potential.

4.7 Torque transfer

The pulley is a 21T5/25-2 made of aluminium with zinc plated steel flanges drives the second link. It is press fitted onto the upper shaft. This pulley transfers torque and must not move in the axial direction. The pulley is shown in Figure 68.

Figure 68 Pulley on the upper shaft

The pulley came with a pilot bore hole diameter of 6 mm, while the shaft had an 8 mm diameter. Therefore, the pulley was drilled to have an ID (inner diameter) of 8 mm diameter. The pulley transfers a torque of maximum 3 Nm with no forces acting in its axial direction. Resulting in there only being tangential shear stress. The parameters required to compute if the press fit can transfer the torque is given in Table 10.

Table 10 Belt pulley press fit values

Parameter	Unit	21T5/25-2	Stainless steel shaft
Material	-	Aluminium	Stainless steel
Axial force	$[N]$	-	-
Torque	$[Nm]$	3	3
OD	$[mm]$	40	8,13
ID	$[mm]$	8	-
Width	$[mm]$	21	-
Young's modulus	$[GPa]$	77,4	196
Poisson's ratio	-	0,327	0,289

Using the theory presented in Section 2.4.6 and applying Eq. (26), Eq. (27) and Eq. (28) shear stress applied by the torsional torque is

$$\tau = \tau_t = \frac{M_z}{2\pi r_n^2 h} = \frac{3000\ Nmm}{2\pi * 4^2 mm^2 * 21\ mm} = 1{,}4\ MPa \tag{74}$$

the shaft influence coefficient by Eq. (33) is

$$\alpha_a = 4{,}0 * 10^{-5} \frac{mm^3}{N} \tag{75}$$

the bore influence coefficient by Eq. (31) is

$$\alpha_n = 7{,}3 * 10^{-5} \frac{mm^3}{N} \tag{76}$$

and the contact pressure by Eq. (29) is

$$p = \frac{(8{,}13 - 8{,}00)mm}{2 * (1{,}42 + 8{,}02) * 10^{-5} \frac{mm^3}{N}} = 575\ MPa \tag{77}$$

The no slip condition for a press fit is given by Eq. (25), and compares the shear stress against the friction coefficient μ multiplied by the contact pressure. If friction coefficient between aluminium and stainless steel is assumed to be the same as the friction coefficient between aluminium and mild steel $\mu = 0{,}61$ [30]. Then Eq. (25) yields

$$1{,}4 \leq 351 \tag{78}$$

Therefore, this press fit will not slip with these values and will be able to transfer 3 Nm of torque.

The worm gear is a BWW08/50/1R and is driving the first link. It is attached by a press fit, as shown in Figure 69.

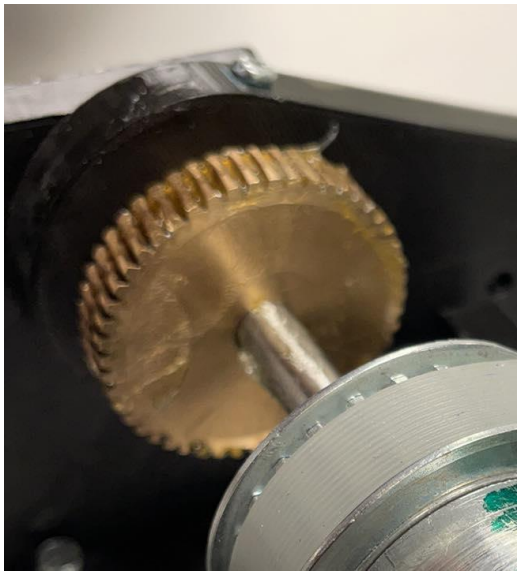

Figure 69 Worm gear press fit

Values required for computing the resulting contact pressure and shear stress is given in Table 11. Note that the Young's modulus and Poisson's ratio for bronze is taken as the averages from [33].

Table 11 Worm gear press fit values

Parameter	Unit	BWW08/50/1R	Stainless steel shaft
Material	-	Bronze	Stainless steel
Axial force	$[N]$	64	64
Torque	$[Nm]$	3	3
OD	$[mm]$	40	8,1
ID	$[mm]$	8	-
Width	$[mm]$	18	-
Young's modulus	$[GPa]$	112	196
Poisson's ratio	-	0,324	0,289

Computing Eq. (27) and Eq. (28) and putting the result into Eq. (26) yields a shear stress of

$$\tau = 1{,}66\ MPa \tag{79}$$

the shaft influence coefficient by Eq. (33) is

$$\alpha_a = 1{,}47 * 10^{-5}\,\frac{mm^3}{N} \tag{80}$$

the bore influence coefficient by Eq. (31) is

$$\alpha_n = 5{,}03 * 10^{-5} \frac{mm^3}{N} \tag{81}$$

and the contact pressure by Eq. (29) is

$$p = \frac{(8{,}10 - 8{,}00)mm}{2 * (1{,}47 + 5{,}03) * 10^{-5} \frac{mm^3}{N}} = 769\ MPa \tag{82}$$

Friction coefficient between stainless steel and bronze is assumed to be $\mu = 0{,}34$ [28]. The no slip condition given by Eq. (25) yields that

$$1{,}66 \leq 769 \tag{83}$$

Therefore, this press fit will not slip with these values and will be able to transfer 3 Nm of torque and 64 N of axial force.

4.8 Failures

As with most projects, there are failures and accidents, and this project is no exception. Three of the failures which cost the most time is

- Buckling of shafts while inserting press fits
- Use of wrong specifications while 3D printing
- Insufficient tolerances for ball bearings.

The buckling which led to the largest loss of time, was the buckling of the shaft which includes the two worm gear pairs, shown in Figure 70. It is clearly shown that the shaft is deformed two places, at the end and the middle section. To gain an understanding of what went wrong it is possible to calculate the force before buckling.

Figure 70 Buckling of shaft

The calculations shown, assume the shaft to have a constant cross-section, implying no other components installed. The shaft measures 140 mm and by using Table 2 to find the effective length factor c, and determine the effective length using Eq. (34)

$$L_{cr} = 1{,}0 * 0{,}14\, m = 0{,}14\, m \tag{84}$$

Critical slenderness by using Eq. (35) is as follows for stainless steel

$$\lambda_1 = \pi \sqrt{\frac{196\mathrm{G}Pa}{671Mpa}} = 53{,}7 \tag{85}$$

and the non-dimensional slenderness using Eq. (36) is

$$\bar{\lambda} = \frac{0{,}14\, m}{\frac{0{,}008\, m}{4}} * \frac{1}{53{,}7} = 1{,}3 \tag{86}$$

Using the red curve in Figure 24, the reduction factor is $\chi = 0{,}35$ and buckling stress is given by Eq. (37)

$$\sigma_{cr} = 0{,}35 * 205\ MPa = 71{,}8\ MPa \tag{87}$$

Force allowed before buckling occurs by Eq. (38)

$$F_{allowed} \leq 71{,}8\ MPa * \frac{\pi}{4} * 8^2\ mm = 3609\ N \tag{88}$$

This implies that force must have exceeded 3609 N for the buckling to happen. The hydraulic press used, shows force applied as tons, where one ton is approximately 9800 N. Therefore, the tons that must have been applied for the buckling to occur is

$$tons\ applied = \frac{3609\ N}{9800\ {}^{N}/_{ton}} = 0{,}37\ ton \tag{89}$$

The calculations above do not consider the other components and as such do not reflect the whole reality. Adding components to this shaft increases the stiffness, and it may be more logical to separate the sections and calculate each of them as individual cases.

Another reason for time lost was the use of incorrect printer specifications for some of the 3D printed parts.

- Link 2 was printed with holes that was too large for the bearings
- Gripper links was printed with 20% infill, resulting in failure
- Some parts which required holes to be drilled were printed with 20% infill, resulting in the drilled holes to be deformed

The gripper was one of the first components to be printed and the first one to fail. It was first printed with 20% infill on all parts, but it became clear that this was not possible. Small components of the gripper did not have the required strength and failed when applying load. The solution was to print small components and components which required drilled holes with 100% infill. Failure is shown in Figure 71.

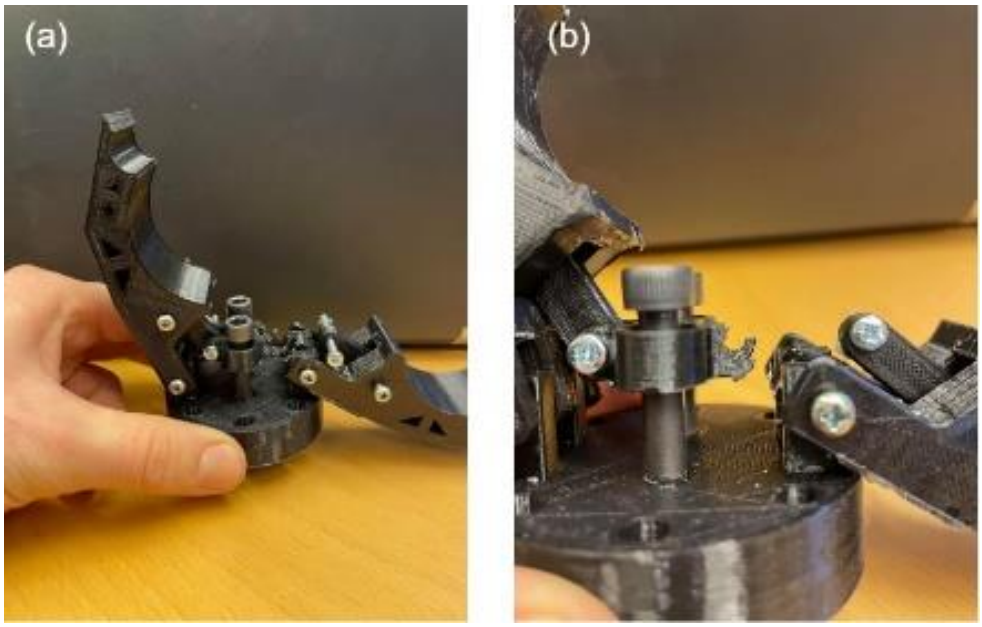

Figure 71 Gripper failure (a) Overview (b) Close up

The third loss of time took a big bite of the budget as well. Having to tight press fits for the ball bearings used on the shafts. The ball bearings are quite small in dimension and is therefore deformed by static loads. It was difficult to achieve perfect press fits and some of them ended up having an interference fit. This led to a high static force when the ball bearing was installed on the shaft and in turn the ball bearing lost its ability to rotate. The ball bearing would only rotate when removed from the shaft. It was clear the tolerance was too tight, and the resulting static force was to high.

An example of the resulting static load of the press fit between the ball bearing 628/8-2Z and a stainless steel shaft is shown in below. Table 12 gives the needed values for calculation of the resulting static force.

Table 12 Ball bearing and shaft dimensions

Parameter	Unit	Ball bearing 628/8-2Z	Stainless steel shaft
Material	-	Steel	Stainless steel
Poisson's ratio	-	0,29	0,289
ID	$[mm]$	8	-
OD	$[mm]$	16	8,1
Width	$[mm]$	5	-
Young's modulus	$[GPa]$	203	196
Static load rating	$[kN]$	1,21	-

Using the equations from Section 2.4.6, the shaft influence coefficient by Eq. (33)

$$\alpha_a = 1{,}45 * 10^{-5} \frac{mm^3}{N} \tag{90}$$

the bore influence coefficient by Eq. (31)

$$\alpha_n = 3{,}99 * 10^{-5} \frac{mm^3}{N} \tag{91}$$

and the contact pressure by Eq. (29)

$$p = \frac{(8{,}1 - 8)\ mm}{2 * (1{,}45 + 3{,}99) * 10^{-5}} = \ 919\ MPa \tag{92}$$

The resulting static force is then simply

$$F = p * contact\ area = 919\ MPa * \ \pi * 8{,}1\ mm * 5\ mm = 116943\ N \tag{93}$$

comparing this to the static load rating from the data sheet of 628/8-2Z ball bearing

$$116{,}94\ kN \gg 1{,}21\ kN \tag{94}$$

Because the static force of the press fit is much higher than the static load from the data sheet, the bearing will deform, and it will not be able to perform as intended. By decreasing the diameter of the shaft, the static load will decrease.

If the parameters in the list below are assumed to be constant

- $\alpha_a = 1{,}45 * 10^{-5} \frac{mm^3}{N}$
- $\alpha_n = 3{,}99 * 10^{-5} \frac{mm^3}{N}$
- $contact\ area = \ \pi * 8 * 5 = 125{,}66\ mm^2$

Then the diameter of the shaft should be less than the equation below to achieve a static load that is within the data sheet specifications

$$d = \frac{2C(\alpha_a + \alpha_n)}{contact\ area} + diameter\ bore \tag{95}$$

Inserting values into Eq. (95) yields that the diameter should be lower than

$$d = \frac{2 * 1210\ N * (1{,}45 + 3{,}99) * 10^{-5}\ \frac{mm^3}{N}}{125{,}66\ mm^2} + 8\ mm = 8{,}001\ mm \tag{96}$$

to not deform the ball bearing. As a result, the machining done on this shaft was nowhere good enough, and a new one had to be made. Making good press fits requires patience and practice.

5. Conclusion

The manipulator designed and produced in this project can fulfil the tasks in the MATE competition. It was no easy job and required a lot of trial and error. This project was dependent on producing the manipulator. Therefore, mechanical work has been done in the workshop and time spent in the workshop has been significant. Lack of planning and impatience resulted in parts being broken and had to be done twice or more. Doing things right the first time would have reduced the time in the workshop drastically. In hindsight, some of this work should have been outsourced.

The way the manipulator is put together allows it to be used just as good on land as in water. However, movement is limited on land as it relies on the ROV to move in the 3D environment. As of now the manipulator would need to uninstall some parts to replace other broken parts. Improvements would be to make the arm more modular and allow for easy access to replaceable parts, making it more service friendly.

Given more time, making a shell for the arm would be a great feature because rotating equipment should be shielded for safety reasons. Adding another link is an improvement which would give the arm more flexibility on land and in water. If a rotating base is added to the manipulator it would be an example of an articulated arm and would work great on land.

An area of improvement is when both Nema 17 stepper motors run in the same direction, a large force will be applied in the axial direction on the worm gear shaft shown in Figure 72.

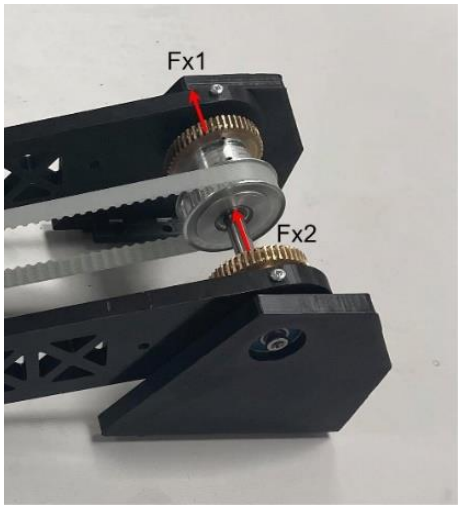

Figure 72 Axial forces on lower shaft

Using the theory presented in Section 2.4.5, this axial force is equal to

$$\sum F_x = 2F_{x2} = 2 * 64\ N = 128\ N \tag{97}$$

While running both worm gears at the same time, the side brackets showed clear signs of movement towards the direction of the axial force. There is room for improvement in this area and this setup should have been made more rigid

The relationship between worm gear pairs and lubricant could have been studied more. The project did not find any studies regarding friction of worm gears whilst submerged in water and assumed the friction coefficients to be the same as in dry conditions. As the worm gear pair is exposed to water, using oil-based lubricant is out of question due to pollution and water-based lubricant would dissolve too quickly. This may be a future study area in the future, as a small reduction in friction in would increase the output torque significantly and therefore increase the lift capacity of the manipulator.

The manipulator is still a work in progress and testing will continue towards the competition and the complete ROV will hopefully work as planned. Only one test at 5-10 m is required for the manipulator and will be performed when the tether is installed on the ROV. It is a good manipulator and UiS Subsea can count on it to work when the competition starts.

The learning curve has been steep, and the frustration level was high at times. Lots of new systems and mechanics were studied, and all the combined knowledge acquired through these three years of education was used. Successfully making a manipulator from scratch has been no easy task, and this project made it possible to get an understanding in how a mechanical engineer works and how to solve the problems that may arise.

.

References

[1] S. Graham, C. Parkinson, M. Chahine and R. Simmon, "Earth Observatory NASA," 2010. [Online]. Available: https://earthobservatory.nasa.gov/features/Water/page1.php. [Accessed 22 February 2021].

[2] R. Capocci, G. Dooly, E. Omerdić, J. Coleman, T. Newe and D. Toal, "Inspection-Class Remotely Operated Vechicles - A Review," *Journal of Marine Science and Engineering*, vol. 5, no. 1, p. 13, 2017.

[3] Worldwide Boat, "Ocean vs Space," [Online]. Available: https://www.worldwideboat.com/news/miscellaneous/ocean-vs-space. [Accessed 22 February 2021].

[4] MATE, "MATE ROV Competition," [Online]. Available: https://materovcompetition.org/. [Accessed 3 February 2021].

[5] Maplesoft, "Maplesoft.com," [Online]. Available: https://www.maplesoft.com/content/EngineeringFundamentals/13/MapleDocument_13/Position,%20Orientation%20and%20Coordinate%20Transformations.pdf. [Accessed 11 February 2021].

[6] Robotic Industries Association, [Online]. Available: https://www.robotics.org/content-detail.cfm/Industrial-Robotics-News/What-is-an-End-Effector-and-How-Do-You-Use-One/content_id/9134. [Accessed 11 February 2021].

[7] Oceaneering, "ROV Systems," Oceaneering, [Online]. Available: https://www.oceaneering.com/rov-services/rov-systems/. [Accessed 26 February 2021].

[8] MATECenter, "2020 EXPLORER class fly-through," 2020. [Online]. Available: https://www.youtube.com/watch?v=KWNBOUqVIPQ. [Accessed 3 February 2021].

[9] T. Reilstad and W. Evje Nodland, “Beregning og styring av manipulator for fjernstyrt undervannsfarkost,” Universitetet i Stavanger, Stavanger, 2015.

[10] C. I. Sjonsti and O. Øverland, “Produktutvikling av elektrisk manipulator til ROV,” Universitetet i Stavanger, Stavanger, 2015.

[11] M. F. Bruset and B. Øygarden, “Design, kinematic analysis and (multibody) simulation of manipulator mechanism for underwater robot (using ADAMS),” Universitetet i Stavanger, Stavanger, 2015.

[12] M. Birkeland, “Product development and testing of tools for ROV,” Universitetet i Stavanger, Stavanger, 2015.

[13] K. Robotics, "Kawasaki Robotics," 04 Oct 2018. [Online]. Available: https://robotics.kawasaki.com/ja1/xyz/en/1803-01/. [Accessed 14 Apr 2021].

[14] R. N. Jazar, Theory of Applied Robotics : Kinematics, Dynamics, and Control (2nd Edition), New York, NY: Springer US : Imprint: Springer, 2010.

[15] Tekkotsu Robotics, "http://www.tekkotsu.org/," [Online]. Available: http://www.tekkotsu.org/Kinematics.html. [Accessed 20 April 2021].

[16] SKF, "SKF Bearing select," SKF, [Online]. Available: https://www.skf.com/group/support/engineering-tools/bearing-select. [Accessed 15 May 2021].

[17] KHK Gears, "KHK Gears," KHK Gears, 2015. [Online]. Available: https://khkgears.net/new/gear_knowledge/gear_technical_reference/gear_forces.html. [Accessed 23 February 2021].

[18] H. G. Lemu, Dimensjonering av maskinelementer, Stavanger: UiS - Institutt for konstruksjonsteknikk og materialteknologi, 2020.

[19] PUREST (Promotion of new Eurocode rules for structural steels), "Designing in stainless steel - Student presentation," February 2018. [Online]. Available: http://www.steel-stainless.org/designmanual. [Accessed 31 March 2021].

[20] S. Meyer, "Step motors take a step in the right direction," 6 March 2015. [Online]. Available: https://www.motioncontroltips.com/step-motors-take-step-right-direction/. [Accessed 4 April 2021].

[21] M. Haldorsen and E. Baloku, "Motor, styring-og reguleringssystem av fjernstyrt undervannsfartøy og manipulatorarm," Universitetet i Stavanger, Stavanger, 2021.

[22] MSC Software, "Hexagon MSC Software," [Online]. Available: https://www.mscsoftware.com/product/adams. [Accessed 20 April 2021].

[23] MSC Software, "Hexagon MSC Software," June 2016. [Online]. Available: http://files.mscsoftware.com/sites/default/files/wp_robotics_ltr_w.pdf. [Accessed 20 April 2021].

[24] RS PRO, "Product datasheet PLA," [Online]. Available: https://docs.rs-online.com/3ffb/0900766b8157cea6.pdf. [Accessed 1 April 2021].

[25] MatWeb, “Overview of materials for Aluminium alloy,” [Online]. Available: http://www.matweb.com/search/DataSheet.aspx?MatGUID=ab8aeb2d293041c4a844e397b5cfbd4e. [Accessed 28 April 2021].

[26] T. Editors of Encyclopaedia, “Stainless steel,” Encyclopedia Britannica, 7 May 2021. [Online]. Available: https://www.britannica.com/technology/stainless-steel. [Accessed 12 May 2021].

[27] MatWeb, “Overview of materials for Stainless Steel,” [Online]. Available: http://matweb.com/search/DataSheet.aspx?MatGUID=71396e57ff5940b791ece120e4d563e0&ckck=1. [Accessed 28 April 2021].

[28] MatWeb, “Overview of materials for Medium Carbon Steel,” [Online]. Available: http://www.matweb.com/search/DataSheet.aspx?MatGUID=098700ed63b24b14bd3bfdbec937489f&ckck=1. [Accessed 28 April 2021].

[29] Engineers Edge, "Coefficients of friction," [Online]. Available: https://www.engineersedge.com/coeffients_of_friction.htm. [Accessed 21 April 2021].

[30] M. Al-Fetyani, "Plot workspace of n-DOF planar robot, MATLAB Central File Exchange," 2019. [Online]. Available: https://www.mathworks.com/matlabcentral/fileexchange/71136-plotworkspace-plot-workspace-of-n-dof-planar-robot. [Accessed 23 April 2021].

[31] Engineering Toolbox, "Friction and Friction Coefficients," 2004. [Online]. Available: https://www.engineeringtoolbox.com/friction-coefficients-d_778.html. [Accessed 26 April 2021].

[32] Stepperonline, "17HS24-2104S Torque Curve," [Online]. Available: https://www.omc-stepperonline.com/download/17HS24-2104S_Torque_Curve.pdf. [Accessed 26 April 2021].

[33] Stepperonline, "14HS20-1504S Torque Curve," [Online]. Available: https://www.omc-stepperonline.com/download/14HS20-1504S_Torque_Curve.pdf. [Accessed 27 April 2021].

[34] MatWeb, “Overiew of materials for Bronze,” [Online]. Available: http://www.matweb.com/search/DataSheet.aspx?MatGUID=66575ff2cd5249c49d76df15b47dbca4&ckck=1. [Accessed 13 May 2021].

[35] R. Vaughn, "MachineDesign," 2013. [Online]. Available: https://www.machinedesign.com/mechanical-motion-systems/article/21831692/the-difference-between-cartesian-sixaxis-and-scara-robots. [Accessed 10 Feb 2021].

[36] Det Norske Veritas, "DNV No 30.1," July 1995. [Online]. Available: https://vdocument.in/reader/full/dnv-no-301. [Accessed 31 March 2021].

Appendix A

Analysing MATE EXPLORER manual

Starting point of any design is to identify what needs to be solved and break the problems into smaller subproblems. This will give an overview of which parts will be necessary for each set of subproblem.

Notes

- Should the company decide to use fluid power, there are requirements and a fluid power quiz that needs to be passed. UiS Subsea decided to make a fully electrical ROV, and therefore fluid power requirements are not described here
- As of writing this, deadlines have been delayed and therefore the pre-study report is not accurate anymore
- New for 2021 is the option to compete in telepresence

General

Within every competition there are some general requirements and constraints. This year 2021 will have the same tasks as the 2020 competition, the reason being that the 2020 competition was cancelled due to COVID-19.

MATE challenges each competitor to think of themselves as entrepreneurs where MATE and the global community is the client. Therefore, UiS Subsea is registered in the Brønnøysund Register. Figure 73 shows the overall structure of the company.

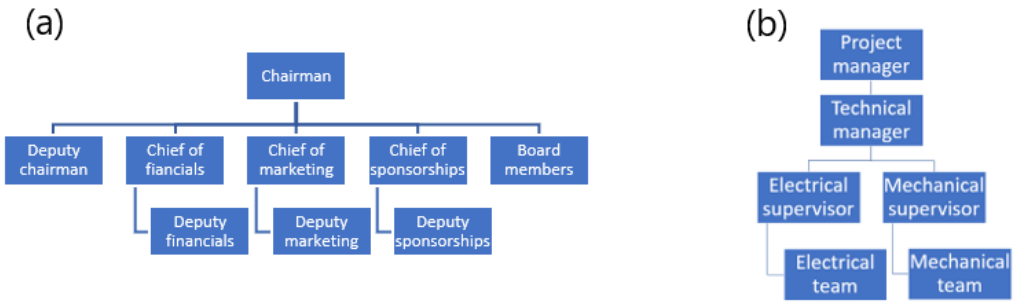

Figure 73 (a) Company structure, (b) Project team structure

Company safety review is to be submitted before the 1st of July. Relevant documentation for the manipulator is

- All waterproof housings are to be documented down to a depth of at least 7 meters
- All sharp edges and elements are removed

It should also include documentation regarding hydraulics, pneumatics, electrical equipment, and other safety specifications. If the company participates with elements that do not pass safety review and safety inspection, the company will be disqualified. If using standard waterproof motors, which are documented to be waterproof by the manufacturer, one can submit the datasheet from the manufacturer. If making waterproof housings or dipping BLDC motors in epoxy, these needs to be tested and documented.

Each team must submit a video demonstration before the 13th of June if competing in person, or by 15th of July if competing in telepresence, this should show the following

- Ability of ROV to perform specific tasks
- The ROV meets the design, build and safety specifications of MATE

In short it must also include video of the power supply, fuses, hydraulics/pneumatics, tether with strain relief, waterproof capsules, no sharp elements, and shrouded propellers.

This implies that the manipulator needs to be done at a minimum of one week before the 13th of June or 15th of July, as the manipulator is crucial for the demonstration. It is possible to make minor changes after the video submission, such as removing/adding buoyancy, adding minor tools or safety applications. However, the system must stay the same and therefore also the manipulator.

Operating environment for the competition will be a pool with:

- Fresh chlorinated water with temperatures between 15º C and 30º C
- Water that should be considered conductive of electrical currents
- Normal light conditions
- No intentional water currents
- Smooth bottom

This is a regular pool, and this reveals why the motors needs to be waterproof as the water is conductive.

Size and weight requirements are as follows:

- Maximum diameter of 92 cm, both in length and height
- Maximum weight of 35 kg

If the ROV is below these requirements, there are extra points to be scored. If exceeding these requirements, the company is disqualified.

All pipes are made of PVC (Polyvinylchloride), which is a type of plastic with a density of approximately $1{,}38\,\frac{g}{cm^3}$.

PVC pipes are measured regarding the size of their ID. The manipulator needs to grab on to the OD, see Table 13 for unit conversion between the relevant sizes.

Table 13 Pipe diameter unit conversion

ID [in]	OD [in]	OD [mm]
0.500	0.840	21.336
1.000	1.315	33.401
2.000	2.375	60.325
3.000	3.500	88.900

Electrical requirements have been handled by the electrical team and therefore this report is not going to deep into these. In short these are:

- Max voltage of 48 V over the ROV
- Max current 30 A
- Power budget 1440 W
- Wires should be secured and laid out with proper workmanship

Task specific

Tasks for 2021 are split into 3 main categories with their respective subcategories.

1. The ubiquitous problem of plastic pollution
    a) Disconnect the power to a Seabin
    b) Replace an old mesh catch bag on the Seabin with a new one
    c) Reconnect the power to a Seabin
    d) Remove floating plastic debris from the surface
    e) Remove a ghost net from midwater
    f) Remove plastic debris from the bottom
2. The catastrophic impact of climate change on coral reefs
    a) Fly a transect line over a coral reef
    b) Map points of interest on the reef
    c) Determine the health of a coral colony by comparing its current condition to past data
    d) Remove coral fragments from the nursery structure
    e) Outplant coral fragments into the reef
    f) Cull an outbreak of Crown of Thorn sea stars
    g) Collect samples of sponge species for pharmaceutical research

3. Maintaining healthy waterways part 2: Delaware river and bay
    a) Deploy a device into the pipe to collect a sediment sample
    b) Determine the type of contaminants present in the sediment sample
    c) Deploy a quadrat to estimate the number of mussels in a mussel bed
    d) Estimate the total amount of water filtered by the mussel bed
    e) Remove a trap full of eels
    f) Place an empty eel trap in the designated area
    g) Create a photomosaic of a subway car submerged to create an artificial reef

Tasks will now be referred to as a number followed by their respective letter. Example: 3a or 1f. Below in Table 14 each task is evaluated whether a manipulator is needed or not based on only the list above. “x” implies a manipulator is needed.

Table 14 Manipulator evaluation

1a	1b	1c	1d	1e	1f	2a	2b	2c	2d	2e	2f	2g	3a	3b	3c	3d	3e	3f	3g
x	x	x	x	x	x				x	x	x	x	x		x		x	x	

Table 15 shows each of these tasks with their respective maximum scores and notes regarding crucial information and how the points are distributed.

Table 15 Point distribution for MATE tasks

Task	Points	Notes
1a	5	
1b	20	
1c	20	Requires a new power connector
1d	15	6 ping-pongs – 15 points 3-5 ping-pongs – 10 points 1-2 ping-pongs – 5 points
1e	20	
1f	10	5 points for each zip-lock bag
2d	10	5 points for each removal of coral fragments
2e	10	5 points for each coral fragments out planted
2f	10	5 points for each culled Crown of Thorn sea star
2g	15	10 points for collecting a sponge 5 points for returning a sponge to the side of the pool
3a	35	25 points for deploying the device 10 points for returning the device to the side of the pool
3c	5	
3e	10	
3f	10	

After each task has been quickly evaluated, more specific info regarding each of these tasks needs to be considered, therefore the next section will show each task with figures and a step by step procedure for execution. Figures are taken from the MATE mission video [8].

1a) Disconnect the power to a Seabin, Figure 74

- A ½ in pipe is acting as a grab point
- Disconnect Seabin power connector by lifting it vertically
- Bring the connector to the side of the pool
- Weight is less than 5 N

Figure 74 Task 1a

Comment:

One can choose whether to grab the connector by the handles or somewhere else.

1b) Replace an old mesh catch bag on the Seabin with a new one, Figure 75

- A ½ in pipe is acting as a grab point
- Remove old mesh catch bag by lifting it vertically
- If debris inside catch bag falls out, one must pick it up
- Return it to the side of the pool
- Install a new one in the same manner
- Weight is less than 5 N

Figure 75 Task 1b

1c) Reconnect the power to a Seabin

This task will require the company to construct a new connector which can supply power to the Seabin, this task will be handled by the electrical team. The task procedure is the same as 1a, just in reverse.

1d) Remove floating plastic debris from the surface, Figure 76

- Remove standard ping-pong balls with the ROV
- Return them to the side of the pool
- Weight is less than 5 N

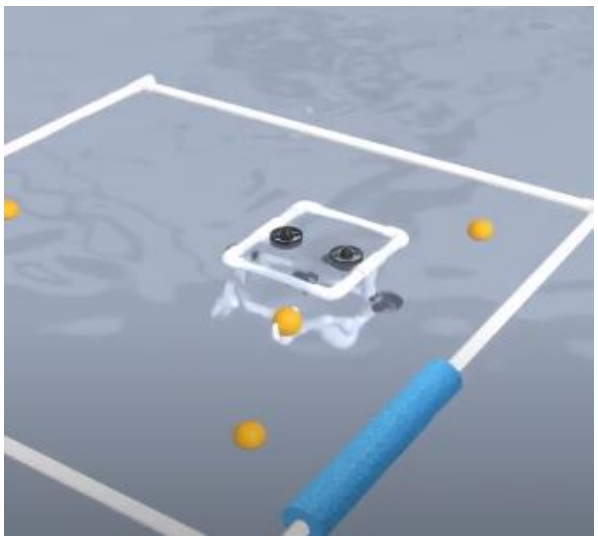

Figure 76 Task 1d

Comment:

The competition video shows a ROV using the manipulator for picking up floating ping pong balls. This may not be realistic. Companies are free to use other equipment if it is attached to the ROV, and it may not be necessary with a manipulator that can grab these.

1e) Remove a ghost net from midwater, Figure 77

- Pull out 5 mm pin to release the net
- Bring the pin to the side of the pool
- A ½ in pipe is acting as a grab point on the net
- The net is positively buoyant
- Bring the net to the poolside
- Weight is less than 5 N

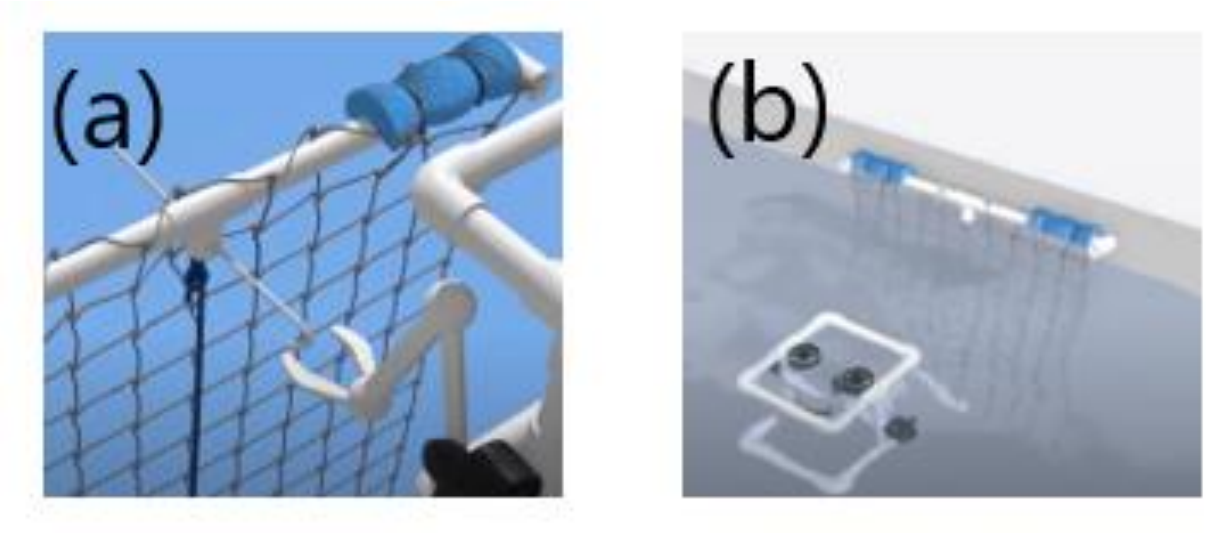

Figure 77 Task 1e (a) Pull out pin, (b) Bring net to the poolside

Comment:

This task is essentially split into two, first remove the pin and return it to the side of the pool, then remove the net and return this as well.

1f) Remove plastic debris from the bottom, Figure 78

- Two 1-gallon bag zip-lock bag
- A ½ in pipe is providing weight so the bag does not drift away
- It will be open
- Pick up the bag
- Bring it to the side of the pool

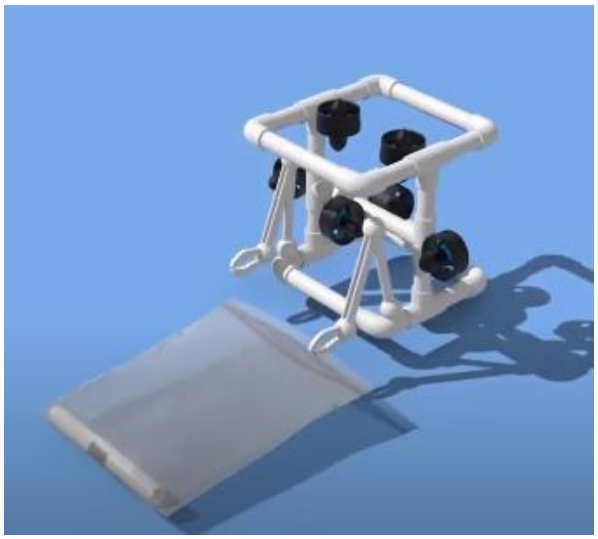

Figure 78 Task 1f

Comment:

If it is possible, grab onto the bottom end of the bag to prevent it from filling up with water. An open bag will create more drag and therefore apply a higher load than a closed one.

2d) Remove coral fragments from the nursery structure, Figure 79

- A ½ in pipe is acting as a grab point
- Remove the coral by lifting it vertically
- Hold it tight
- Weight is less than 5 N

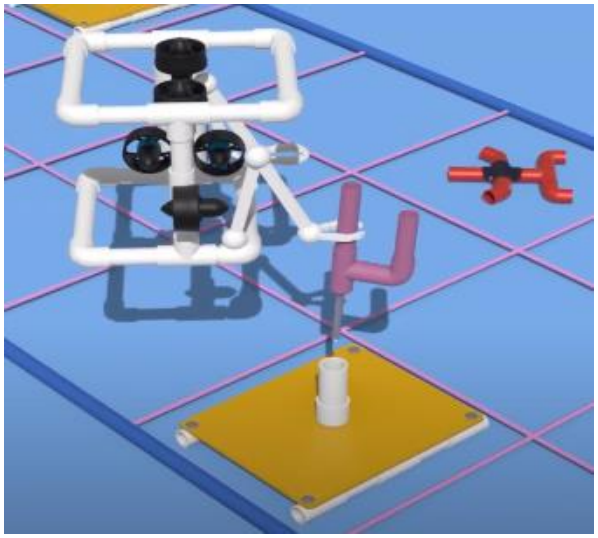

Figure 79 Task 2d

2e) Out plant coral fragments into the reef

After completing 2d, move over to new destination while holding the coral and then perform 2d in reverse. No further specifications needed.

2f) Cull an outbreak of Crown of Thorn sea stars, Figure 80

- ½ in pipe with a square of 4 x 4 cm with Velcro hooks
- Rope acting as a grab point
- Place this on the sea star lying flat on the bottom
- The sea star has a square of 5 x 5 cm with Velcro loops

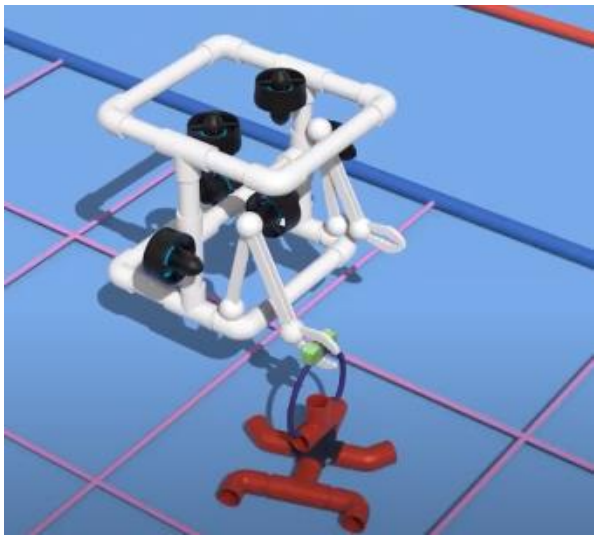

Figure 80 Task 2f

Comment:

Precise placement is required for the Velcro to attach. The end effector must be able to completely close its jaws for the rope to not slip.

2g) Collect samples of sponge species for pharmaceutical research, Figure 81

- 2 in pipe is acting as a grab point
- Three 2 in couplings will be stacked
- Remove the top one without the others being knocked over

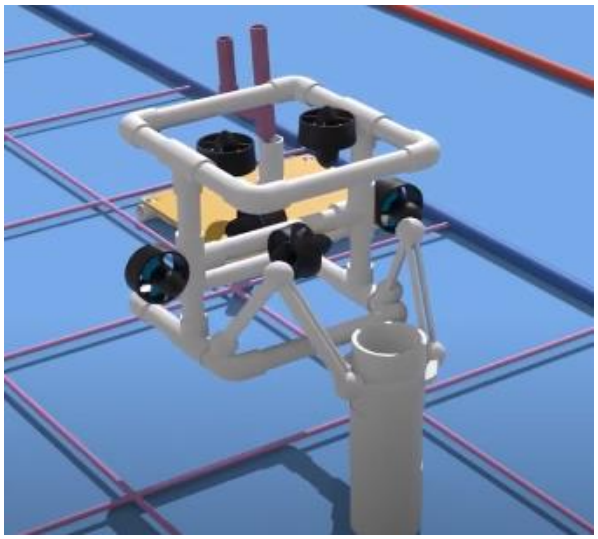

Figure 81 Task 2g

Comment:

This is the only task which has a grab point of 2 in diameter.

3a) Deploy a device into the pipe to collect a sediment sample, Figure 82

- Pull out the mini-ROV from the pipe
- Grab point not specified
- Return it to the side of the pool with the sample it has collected
- Weight is less than 5 N

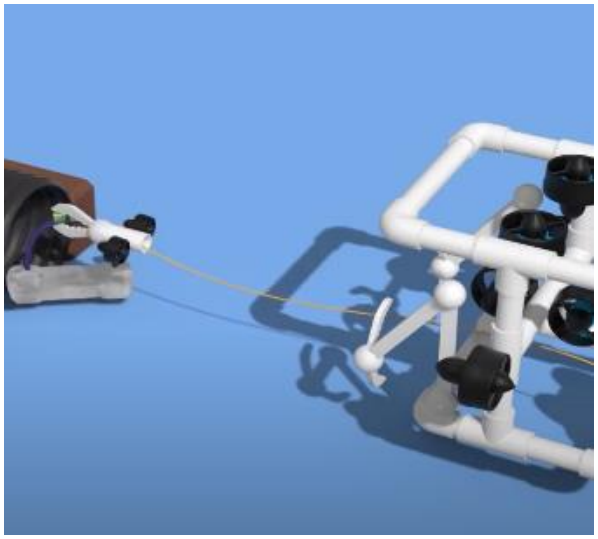

Figure 82 Task 3a

Comment:

This device may be a mini ROV or something else entirely. Most options will require the manipulator to grab the sample and return it to the side of the pool, therefore the device should have a good grab point.

3c) Deploy a quadrat to estimate the number of mussels in a mussel bed, Figure 83

- ½ in pipe is acting as grab point
- The frame is a 50 x 50 cm square
- Lay it flat on the bottom

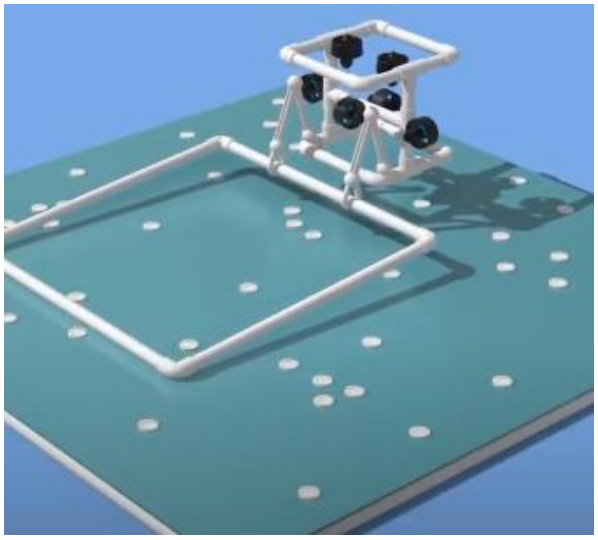

Figure 83 Task 3c

Comment:

If using one manipulator instead of two, it is crucial to grab onto the middle of the frame. Failure to grab the middle will result in an unnecessary moment on the manipulator and ROV.

3e) Remove a trap full of eels, Figure 84

- #U310 Bolt is acting a grab point
- Return the full trap to the side of the pool
- Empty the trap

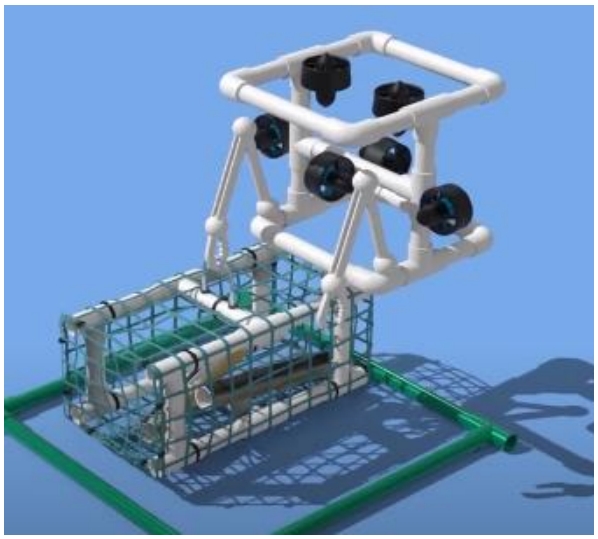

Figure 84 Task 3e

3f) Place an empty eel trap in the designated area

Continuation of 3e, and the only step is to bring the empty trap back into the designated area.